THERMO-MECHANICAL MODELLING OF HOT FLAT-ROLLING OF COMPONENTS WITH CURVED PROFILES

By

Ming Xiao

B. ASc. (Electronic-Mechanical Engineering)

Guilin Electronic Industry College, 1984

A THESIS SUBMITTED IN PARTIAL FULFILLMENT OF

THE REQUIREMENTS FOR THE DEGREE OF

MASTER OF APPLIED SCIENCE

in

THE FACULTY OF GRADUATE STUDIES

MECHANICAL ENGINEERING

We accept this thesis as conforming

to the required standard

THE UNIVERSITY OF BRITISH COLUMBIA

June 1993

In presenting this thesis in partial fulfilment of the requirements for an advanced degree at the University of British Columbia, I agree that the Library shall make it freely available for reference and study. I further agree that permission for extensive copying of this thesis for scholarly purposes may be granted by the head of my department or by his or her representatives. It is understood that copying or publication of this thesis for financial gain shall not be allowed without my written permission.

Mechanical Engineering
The University of British Columbia
2075 Wesbrook Place
Vancouver, Canada
V6T 1Z1

Date: June 1993

ABSTRACT

A complete mathematical model for implementing the VGR process(a flat rolling process for producing components with variable thickness) under hot working conditions has been established. The work is based on an idea that a combination of separate submodels, such as, deformation, flow stress, roll force, temperature, etc., should be used, so that new development in each of these areas can be easily incorporated.

A deformation submodel, based on the upper bound theorem, is given for the analysis of three-dimensional deformation of the workpiece. A simple velocity field is proposed. To preserve the theoretical consistency, an equivalent coefficient of friction is adopted for the roll force calculation. Furthermore, the basic assumption, i.e., the rigid perfectly-plastic material assumption, is modified by introducing a concept of an isotropic rate-dependent material. Satisfactory results were obtained in spread, torque and force prediction.

To obtain the mean temperature of the workpiece, a temperature submodel is formulated based on one-dimensional transient flow in the roll-bite and two-dimensional flow outside the roll-bite. The model is capable of predicting the through-thickness temperature distribution in the roll-bite, estimating the mean temperature of the deforming body, and roughly calculating the mean temperature distribution along the workpiece.

To characterize the high temperature behaviour of steels, the well-known unified creep relationship is chosen as the flow stress submodel. Reasonably accurate prediction of the flow stress is achieved by using some experimental data reported in the literature.

Table of Contents

List of Figures

Notation

$0, 1$	subscripts for entrance and exit, respectively
i, f	subscripts indicating the initial and final conditions
A_s	surface area of the workpiece, m^2
B	Stefan-Boltzmann constant, $5.67\times\ 10^{-8}$ $Wm^{-2}K^{-4}$
C	control parameter in the roll gap function
C_w	specific heat of the workpiece, $Jkg^{-1}K^{-1}$
$\dot{E}_d, \dot{E}_f, \dot{E}_s$	energy dissipation rates due to deformation, friction and shear, respectively
F	roll separating force
F_T	frictional force at the interface between rolls and workpiece
F_R	overall radial force on the roll
$G(C)$	the roll gap function
h_c	convection heat transfer coefficient
$h(x)$	the thickness function
$H(\tau)$	heat transfer coefficient
J^*	upper-bound on power
k	the shear yield stress
k_s	thermal conductivity of the workpiece, $kWm^{-2}K^{-1}$
l	the length of the projected arc in contact
m	friction shear factor
q	heat generation
Q	the prescribed flow factor

Q_a	activation energy, kJ/mol
r	the reduction ratio: $r = (t_0 - t_1)/t_0$
R_g	the universal gas constant, 8.31 J/mol K
R	roll radius
t	the thickness function
M	the rolling torque
T	constant temperature, with different subscripts (used in Chapter 5)
T_r	roll surface temperature, °C
T_s	surface temperature of the workpiece, °C
$T(x, \tau)$	temperature field in workpiece, °C
V	volume of the workpiece
V_R	roll peripheral velocity
V_x, V_y, V_z	velocity components in the x, y, z directions
$w(x)$	the width function
x_n	neutral point
ΔV	velocity discontinuity
ϵ	emmisivity of the workpiece, $\mathrm{Jkg^{-1}K^{-1}}$
$\dot{\varepsilon}_{ij}$	strain rate tensors
$\bar{\varepsilon}$	mean strain
$\dot{\bar{\varepsilon}}$	mean strain rate
μ_{eq}	equivalent coefficient of friction
ρ_w	density of the workpiece, (for steel, 7600 $\mathrm{kgm^{-3}}$)
σ	the flow stress of the material
τ_0	the friction shear stress
τ	time variable

ACKNOWLEDGEMENT

I would like to express my sincere thanks to Professor F. Sassani for taking the author as a graduate student and providing the inspiration for this work. His valuable discussions and helpful suggestions throughout the project are particularly apperciated. I would like to thank Professor I. Yellowly for his suggestion of using the upper bound approach in this work at first place, and his stimulating discussions at the times when I was in need of help.

Financial asistance from NSERC is gratefully acknowledged. I would also like to thank computer system managers, G. Rohling and A. Steeves, for their help in using the computers in the Department.

I wish to express my appreciations for my fellow students (also my friends) in the Department for their constant interactions and encouragement, in particular, Ramin Ardekani and Fariba Aghdasi.

I take this opportunity to express my gratitude for the support and encouragement shown by my parents, to which I am in debt for a lifetime.

TO MY PARENTS

Chapter 1

INTRODUCTION

1.1 Deformation Analysis of Rolling Process — An Overview

The history of the rolling process can be traced to more than four hundred years back, whereas, the theoretical analysis, mainly within the plane-strain assumption, of the process began much later, probably in the 1920's[1].

Apparently because the plane-strain analysis was much simpler and was able to meet the requirements in steel production, the most widely known and used theoretical models to date were derived by assuming plane-strain deformation, such as Orowan's model [1] and Von Karman's equation [1].

Usually, all the earlier passes in the hot rolling of slabs were scheduled by means of empirical methods, and only the few final passes were of greater concern, where the parameters of the products were obtained. In such situations, the plane-strain assumption worked very well, since in most cases, the width-to-thickness ratio of the material in rolling is much larger than 10 and thus the spreads in width can be ignored. It was observed in the operation of the strip mills that the spreads in width seldom exceed 1 to 2 percent[2].

With increasingly stringent demands for accuracy, innumerable efforts have been put into the development of theoretical models for flat rolling during the last seven decades. Almost all the successful comprehensive(namely, various factors were included, and usually also combined hot and cold rolling) models for the strips and plates rolling were

evolved from plane-strain assumption, not only because it was most reasonable, but also because the resulting models were readily adaptable for engineering use and rather convenient for the programming of control computers. It would not be an exaggeration that if one would state that the plane-strain analysis in the rolling process has culminated with the help of the rapid advances in the computer technology in the recent years. Or in other words, if one were seeking a solution to a plane-strain problem in the traditional rolling process, where the roll-gap is constant, most likely he would find out, amongst the vast literature on the related subjects, that the work has already been done for some time.

Although the research and development of the rolling process have reached such a encouraging stage, however, all the theoretical works, including quite a few successful attempts made in the last three decades, where three dimensional deformation analyses were worked out, say, [3-6], were originated from constant roll-gap geometries, for a uniform thickness of the products has been one of the primary goals in flat rolling. Having considered this situation, one may realize that a detailed review on the literature would not be helpful, and therefore is omitted here.

1.2 Manufacturing of Single Leaf Springs

At the beginning of 70's, the automobile industry in Britain began to make tapered leaf springs using the flat rolling process, where the roll-gap was designed as a variable so that it could be changed continuously while rolling and produced a tapered leaf, which had thickness variations along its longitude, figure 1.1a. Ever since, the world-wide demand for the tapered leaf springs has been increasing. The distinct advantage of such a process is its flexibility, in producing an arbitrary set of parameters of the tapered shape, that

can not be achieved by any other tooling structure.

It has been well-known for a long time that the most efficient type of leaf springs is those with a parabolic profile [7], figure 1.1b, but the preparation for such shaped materials is much too difficult. The reason that the industry wound up in the manufacturing of the tapered leaf springs is that the tapered leaf is a compromise between the difficulties involved in the manufacturing and its efficiency.

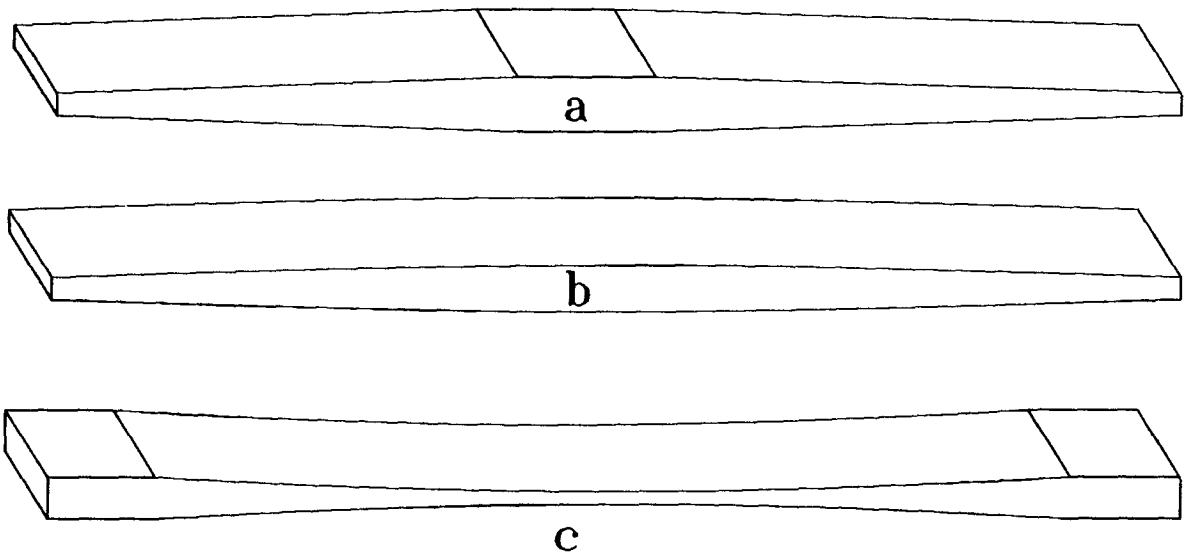

Figure 1.1: The schematic illustration of the profiles of single leaf springs. a. Tapered profile. b. Parabolic profile. c. Arbitrary profile.

Although, in the last two decades, a number of mills were set up around the world specifically for making of the tapered leaf springs, no theoretical work on the subject has appeared in the literature.

The only research work on this subject that one may find out in the literature, [8], [9] and [10], was based on the empirical formula for side spreads prediction, which was originated from factor-analysis in 1950's, proposed by Sparling[11] in 1961 and improved by El-Kalay and Sparling[12] in 1968. It is well-known that empirical formulae are often

simple and handy to use. Chitkara and Johnson[13] found out that the formula gave reasonable results within the range of experimental conditions under which they were devised, "however, their accuracy under different conditions is open to question." The present author considers that it could be a good idea to take advantage of the formula, if the purpose of the research is only to give fair estimates in the deformation, that is, the spreads and the elongation. As a matter of fact, good results in their work were reported[8][9][10]. However, the formula may not be adequate for machine set-up and process design, where a consistent model is needed in order to calculate deformation along with the force and torque variations during production. Moreover, temperature effects are dominant in hot rolling, to which much attention should be given. It would be most desirable to have a model capable of incorporating the most recent developments, say in tribology and material science, so that a thorough knowledge of the deformation and force of the process may be obtained, thereby confidence may be gained for the design purpose.

After a careful study of the important previous works on the flat rolling process, the author believes that any reasonable theoretical analysis of the variable gap rolling (VGR) process[1] has to start with the ever-changing geometry of the workpiece, and one has to give up the idea of making a direct use of any available theoretical models in flat rolling analysis.

1.3 Aim and Approach

As mentioned in Section 1.1, only in cases where the spread in width is negligible, the problems can be considered in plane-strain.

[1]From now on, for the sake of convenience, the rolling process with a variable roll-gap geometry will be referred to as the VGR process.

It is conceivable that two schemes may be used in the design of the production rolling mills for leaf springs. One is that the rolling is to start with a rectangular bar, of which the width-to-thickness ratio may be 1 to 3, as those required by some already existing production mills for tapered leaf springs. In this scheme, the leaf spring is produced one at a time, and the main problems are that the width of leaf must be constant and also the thickness variation is usually from 30% to 70%[14]. Apparently, in such cases the deformation analysis has to be considered in three dimensions, except when considering edge-rolling for the purpose of width correction(see Section 2.1).

The other scheme is to start with a wide slab, the width-to-thickness ratio may be larger than 10. In this case, the slab is to be rolled to the desired dimensions and more than 10 leaves can be obtained at a time by cutting the rolled blank. Accordingly, the spread in width is at least no longer a serious problem, and the process may be considered in plane-strain. However, the machine set-up in this case may be much more costly. Besides, at present, cutting process is usually detrimental to the final properties of the products in terms of their strength and fatigue resistance, and therefore is not preferable in leaf spring production.

The present work is aimed to propose a generic theoretical model, three dimensional strains will be considered. The model should be capable of giving a good description of the variation in deformation, force and torque, under conditions of hot working and varying geometry. Thus, the model may also be used in producing such components shown in figure 1.1c.

Chapter 2

BASIC CONSIDERATIONS

2.1 Available Analytical Methods

In the past half century, a number of approximate analytical methods have been developed and applied to the rolling process, amongst which the most well known are the following.

1. **The slab analysis**

   This method is very restricted by its nature and is usually used for a rough prediction of the required load, with a reasonable stress distribution; but it is not a suitable method for a rigorous deformation analysis.

2. **The slip line field**

   Since its derivation is based on the plane-strain assumption for perfectly plastic materials, generally speaking, it is not reasonable to apply this method to three dimensional problems. In addition, the construction of slip-line fields is still quite limited in predicting results that offer good correlations with experimental evidence[16].

   One of the applications of the method that should be mentioned here is the one used by Hawkyard *et al* [9] in ring-rolling. See figure 2.1. Despite its formidable-seeming complexity, that is, ring-rolling has the similarities with asymmetric rolling processes, it could still be tackled since the work-roll feed rate is generally small and is a known constant. It is worth noting that the reduction is usually very

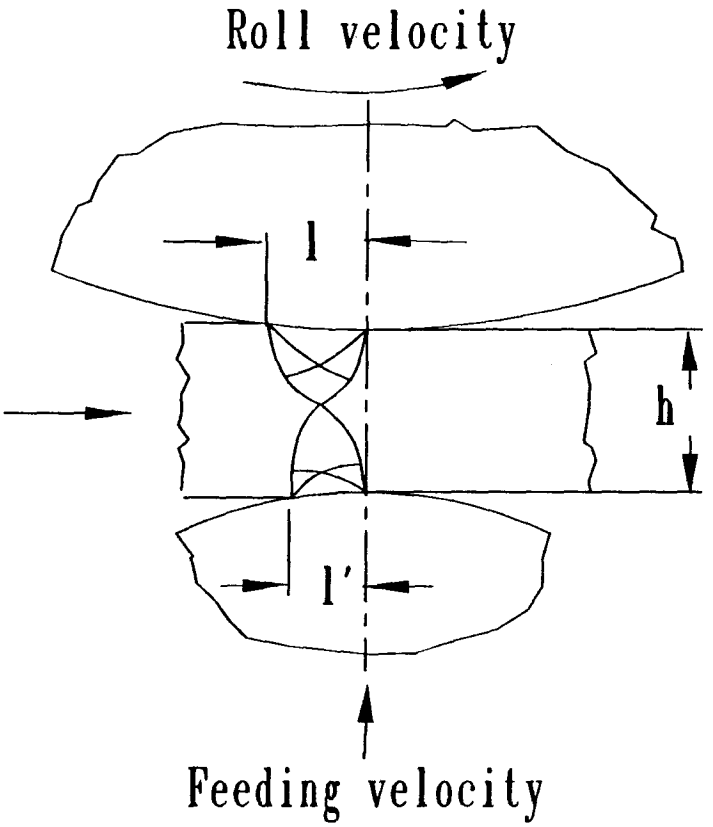

Figure 2.1: The schematic illustration of ring-rolling configuration

small for each turn and the ratio of l/h is usually large, figure 2.1. These lead to such an effect that the plastic deformation between the rolls is far from penetrating the ring thickness, and instead of the usual bulges in rolling, fishtail-shaped sides result, figure 2.2a.

Based on the above observations, they defined the plastic deformation between the rolls by the kind of slip-line field applicable to flat-end rigid tools, which was developed by Hill [17], when forging a block whose depth is larger than that of the tool width, figure 2.2b, was considered.

Apparently, such a method is not applicable to the deformation in the present process, but it may be a good choice for the edge-rolling, which is usually used to obtain a uniform width.

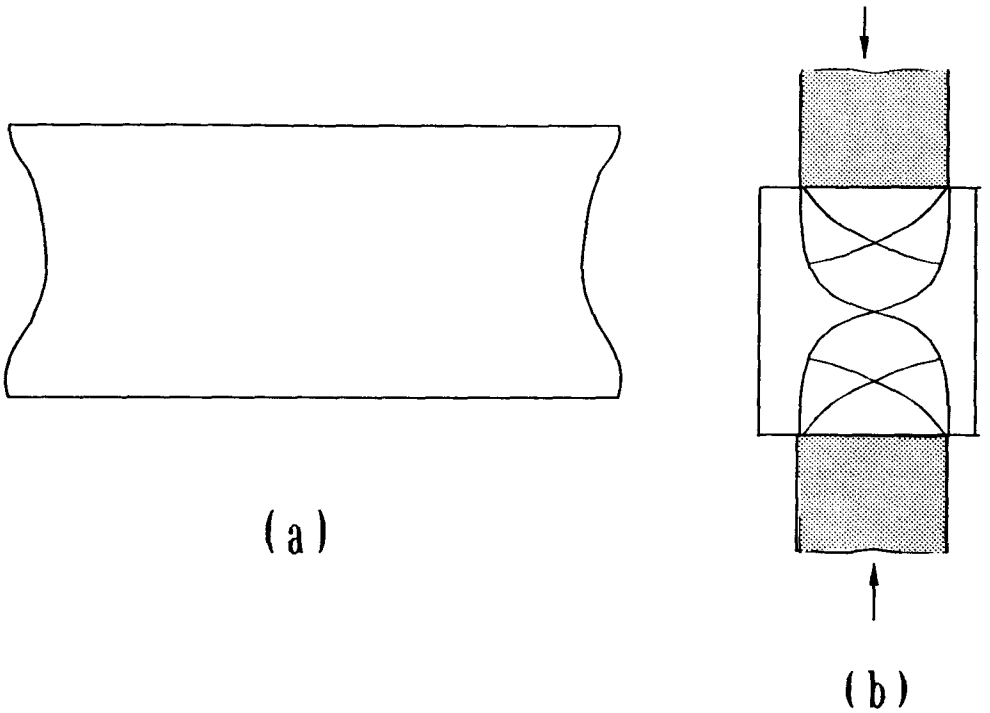

Figure 2.2: (a) The illustration of fishtail-shaped sides in ring-rolling. (b) The illustration of the slip-line field for flat-end tool forging.

3. **The visioplasticity**

   This approach is experimental and could be useful if theoretical or numerical relations cannot be worked.

4. **Hill's general method**[3]

   This method is derived from the virtual work-rate principle, and will be cited in the related part of the next chapter.

5. **The finite-element method(FEM)**

   The applications of this method to the analysis of three dimensional rolling process were started in early 80's [18]. One of the main advantages of the method is that it can provide detailed information, point to point, of the deforming body *between the rolls*, which, however, requires a step-by-step computational procedure and

therefore, requires a much higher data storage and much longer computing time. Fortunately, the conventional rolling process is a steady-state process, and only a few samples of the deformation analysis are needed to obtain a good prediction of the whole process.

The formidable difficulty in the analysis of the VGR process is that the pattern of the deformation between the rolls changes continuously throughout the process, and inevitably, a calculation for every point along the product has to be done. For instance, to roll a one-meter long component, the step to generate a set of reasonable interpolation data for the digital controller of the machine is 0.0005 meter, then, at least 2000 steps is needed (for one pass), which means that if finite-element method were to be used, the demands for data storage and computing time would increase a thousand times! Incidentally, Grober [19] reported in 1986 that a simulation of *transient* hot rolling of steel was performed, where a CPU time of 7 hours on a microVAX II computer was consumed for the simulating of a total length of 51.25 mm, and only a two-dimensional finite-element model was used. This, most likely, were the very reason that no significant theoretical work on the subject, ie., the VGR process, by using FEM (nor by any other method) was found in the English publications(a rather great amount of efforts has been put into the search). Conscious of the foreseeable great demands for the computation, the method is not to be used in the present problem.

6. The upper bound approach (UBA)[1]

The upper bound approach is valuable to mechanical or production engineers, since it offers rather good results in the roll mill operations with lower costs, and from the viewpoint of machine design, the data produced by the method, though somewhat

[1]This name was first used by W. Johnson and was considered being well-expressed[55].

approximate in nature, are certainly on the safe side. It can also be found in the literature that many researchers used this approach in conjunction with other methods, such as least squares, finite-element, viscoplasticity and the weighted residuals, etc., with which the difficulties to obtain proper velocity fields may be reduced.

Perhaps the earliest application of the UBA to the three dimensional analysis of the conventional rolling process was made by Oh and Kobayashi in 1975[5], where quite accurate solutions to the average spread and the torque requirements were given. By extending the work of Oh and Kobayashi[5], Lahoti, *et al*, developed a production software package for the rolling of plates and airfoils in 1978 [20], and Sevenler, *et al*, managed to analyze shape rolling with flat rolls [21]. With the method, bulge predictions were also attempted by Kennedy[6] in 1986, though fairly noticeable difference between the theoretical predictions and the experimental results, cited in the work, exists. The major difference between the model by Oh and Kobayashi[5] and the one by Kennedy[6] is that two totally different solutions to the velocity fields were used.

Considering all the facts involved, it is reasonable to use the upper bound approach in the analysis of the present problem.

2.2 Assumptions

The present analysis is based on the mathematical consideration proposed by C. S. Yih [22] in 1957. To be practical, the following assumptions have to be made.

1. The material is isotropic and incompressible.

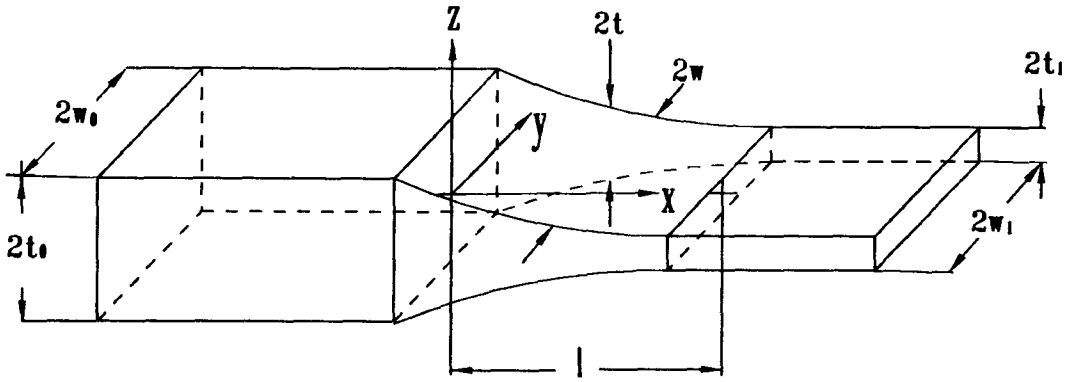

Figure 2.3: Schematic illustration of the part of a bar in rolling

2. The material assumes perfect rigid-plastic properties, that is, the flow stress of the material σ is constant[2].

3. The deformations meet Mises yield criterion and assume unrestricted plastic flow, therefore, the Lévy-Mises equations can be used. The inertial forces are negligible, since in this type of rolling lower speeds are used.

4. The friction shear stress τ_0 is constant in the roll-workpiece interface and is given by a constant friction shear factor m defined by the relation, $\tau_0 = m \cdot \sigma/\sqrt{3}$.

5. The bar to be rolled can be considered as a set of flow solenoids with different rectangular cross sections, figure 2.3 shows one such element. For the sake of simplicity, any line in z-direction is assumed to remain straight. Since one can never have the exact solution to the flow patterns in question, good approximation has to be dependent upon two properties — theoretical tenability and mathematical feasibility. In order to avoid overwhelming mathematical difficulty, it would be

[2]This assumption is only based on the strict restraint in the upper-bound theorem. In fact, in real applications, this restriction has to be relaxed and the concept of instantaneous yield conditions has to be adopted. Detailed discussion may be found in Sections 5.2 and 5.3.

better to give up the bulge prediction at this stage.[3]

6. The profile of the product can be expressed in a continuous function or may be defined in several continuous intervals with different functions, and the slopes of the function, have to be very small with no sharp change on the boundaries of the intervals, if any.

2.3 Coordinate Systems

It can be seen that the cartesian coordinate system,(x, y, z), is convenient in developing the velocity fields, figure 2.4. The x, y and z directions are defined along the length, width and thickness of the product, respectively.

For convenience in design and control of the machine, the coordinates (X, Y, Z), figure 2.4, are used. And C is a constant dependent upon the dimensions of the products and the configuration of the rolling mill. Henceforth, the roll gap function can be simply expressed as $G(x + C)$ in the analysis coordinate system (x, y, z).

[3]Actually the author considers that it should be a good choice to make use of the available methods for bulge prediction with this model, amongst which there are several good methods. Besides, the author believes that accurate bulge prediction that is really helpful in production is more an art than a science, by its nature.

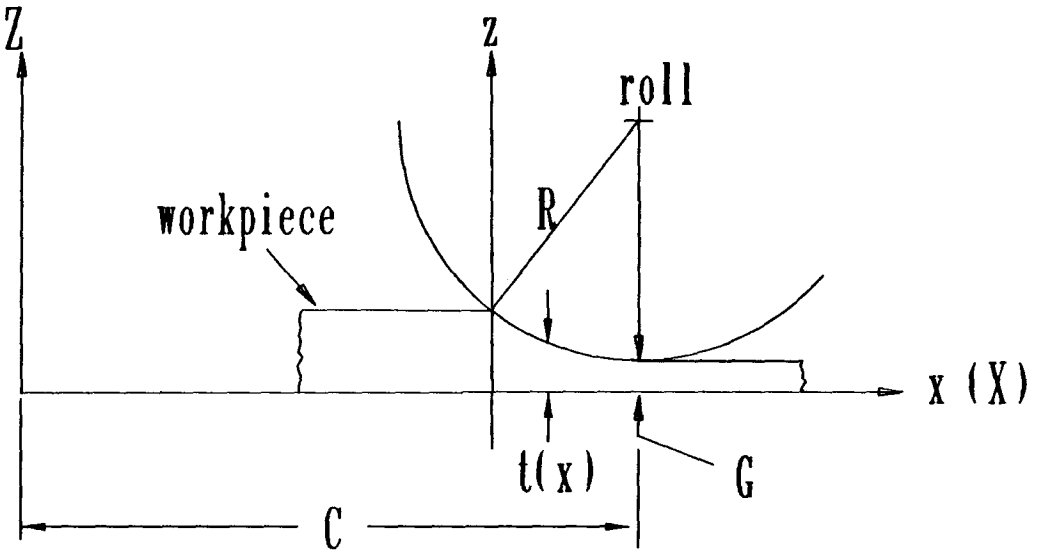

Figure 2.4: The coordinates system

Chapter 3

CONSTRUCTION OF VELOCITY FIELDS

3.1 The Dual-Functional Method

As mentioned Chapter 2, the analysis will start with Yih's mathematical considerations[16], of which the related results are to be re-introduced here, however, detailed discussions should be referred to the original paper.

Yih derived that for a continuous flow, the velocity vector can be expressed as the following:

$$\mathbf{V} = (grad\ f) \times (grad\ g) \tag{3.1}$$

where f and g are two artificially chosen functionals that may represent stream surfaces in which streamlines are embedded, and along any streamline the two functionals assume the following form,

$$f(x, y, z) = a \qquad g(x, y, z) = b \tag{3.2}$$

where a and b are some constants.

In addition, since the tool surface is the actual flow surface, f can be so chosen as to make a solid boundary an f-surface, and g the free sides of the being rolled material and can be solved by the equation,

$$\mathbf{V} \cdot (grad\ g) = 0 \tag{3.3}$$

which is one of the properties of continuous flow.[1]

[1]Yih did not indicate this last approach explicitly, which, however, can be easily derived from the original idea.(See Section 3.2)

3.2 A Brief Derivation of the Solution to the Velocity Fields

Incidentally, a much shorter and simpler mathematical derivation of the aforementioned idea was discovered during this work, which is the following.

Assuming an incompressible material(nondiffusible), the following holds,

$$\frac{\partial V_x}{\partial x} + \frac{\partial V_y}{\partial y} + \frac{\partial V_z}{\partial z} = 0 \tag{3.4}$$

which can be written in the following form,

$$div\ \mathbf{V} = 0 \tag{3.5}$$

Note that we have the following mathematical relationship,

$$div\ (\mathbf{A} \times \mathbf{B}) = \mathbf{B} \cdot (curl\ \mathbf{A}) - \mathbf{A} \cdot (curl\ \mathbf{B}) \tag{3.6}$$

$$curl\ (grad\ \phi) = 0 \tag{3.7}$$

where A, B and ϕ are any differentiable functionals. Suppose that there are two continuous functionals, $f(x, y, z)$ and $g(x, y, z)$, the gradients of which exist. Let

$$\mathbf{A} = grad\ f \qquad \mathbf{B} = grad\ g \tag{3.8}$$

Substituting Eq.3.8 into 3.6, and using Eq.3.7, the following results,

$$\begin{aligned} &div\ [(grad\ f) \times (grad\ g)] = \\ &(grad\ g) \cdot [curl\ (grad\ f)] - (grad\ f) \times [curl\ (grad\ g)] = 0 \end{aligned} \tag{3.9}$$

Comparing Eq.3.9 with 3.5, we have

$$\mathbf{V} = (grad\ f) \times (grad\ g) \tag{3.10}$$

Eq.3.10 suggests that $\mathbf{V}$ could be constructed by two functionals, and the only restraint to these two functionals is that their gradients exist. In other words, f and g

need to be constants. Henceforth, f and g can be artificially chosen. Naturally, f can be chosen as the tool surface, meanwhile, adopting the prescribed flow factor (see the derivations below); and g can be so chosen as to represent the free surfaces of the material. The latter property leads to the following,

$$\mathbf{V} \cdot \mathbf{n} = 0 \tag{3.11}$$

where $\mathbf{n}$ is the normal vector on free surface of the material between the rolls.

Since $\mathbf{n}$ and *grad* g have the same direction, Eq.3.11 can be replaced by

$$\mathbf{V} \cdot (grad\, g) = 0 \tag{3.12}$$

which is the same as Eq.3.3 and can be used to determine g.

3.3 The Derivation of the Velocity Fields

Using the notation of gradient, Eq.3.1 may be written as

$$\mathbf{V} = \begin{vmatrix} \frac{\partial f}{\partial y} & \frac{\partial f}{\partial z} \\ \frac{\partial g}{\partial y} & \frac{\partial g}{\partial z} \end{vmatrix} \mathbf{i} + \begin{vmatrix} \frac{\partial f}{\partial z} & \frac{\partial f}{\partial x} \\ \frac{\partial g}{\partial z} & \frac{\partial g}{\partial x} \end{vmatrix} \mathbf{j} + \begin{vmatrix} \frac{\partial f}{\partial x} & \frac{\partial f}{\partial y} \\ \frac{\partial g}{\partial x} & \frac{\partial g}{\partial y} \end{vmatrix} \mathbf{k} \tag{3.13}$$

where **i, j, k** are unit vectors along x, y and z directions, respectively. Thus, the velocity fields can be expressed as the following.

$$\begin{aligned} V_x &= \frac{\partial f}{\partial y}\frac{\partial g}{\partial z} - \frac{\partial f}{\partial z}\frac{\partial g}{\partial y} \\ V_y &= \frac{\partial f}{\partial z}\frac{\partial g}{\partial x} - \frac{\partial f}{\partial x}\frac{\partial g}{\partial z} \\ V_z &= \frac{\partial f}{\partial x}\frac{\partial g}{\partial y} - \frac{\partial f}{\partial y}\frac{\partial g}{\partial x} \end{aligned} \tag{3.14}$$

With the idea described in previous Section in mind, it can be easily understood that the assumption 5 in Section 2.2 is theoretically tenable. The remaining problem will be

to choose the proper functionals, f and g, which should assume the simplest forms but satisfy Eq.3.3.

As indicated earlier, the functional f can be chosen as the tool surface. From figure 2.4, under assumption 5 the roll surface can be taken as part of a cylinder, and expressed as

$$z = t(x) = G(x \pm C) + R - \sqrt{R^2 - (l - x)^2} \tag{3.15}$$

Obviously, t(x) is a non-zero function in this case and Eq.3.15 therefore can be written as

$$\frac{z}{t(x)} = 1 \tag{3.16}$$

Since we are talking about flow, it will be seen that to relate Eq.3.15 to the roll peripheral velocity at this stage is a reasonable choice (also see next section), thus, Eq.3.16 becomes

$$\frac{Qz}{t(x)} = Q \tag{3.17}$$

where Q is an arbitrary constant related to the flow and its physical meaning will turn out later.

Now define

$$f(x, y, z) = \frac{Qz}{t(x)} \tag{3.18}$$

which then meets the restraint that f should be a constant.

Before using Eq.3.3 to determine functional g, some explanation relating to the assumption 5 should be given. As can be seen in figure 3.1, $g(x, y, z)$ is assumed as the flow surfaces constituted by the free sides of the part of a bar being rolled and are parallel to z-direction. Note that the curvature of the sides is usually very large (the dotted line in figure 3.1) in reality and very close to a straight line (the solid line in figure 3.1), which may be confirmed by many photographs in the literature reflecting the deformation of the workpiece between the rolls that showed the projected profiles in the x-y plane remain

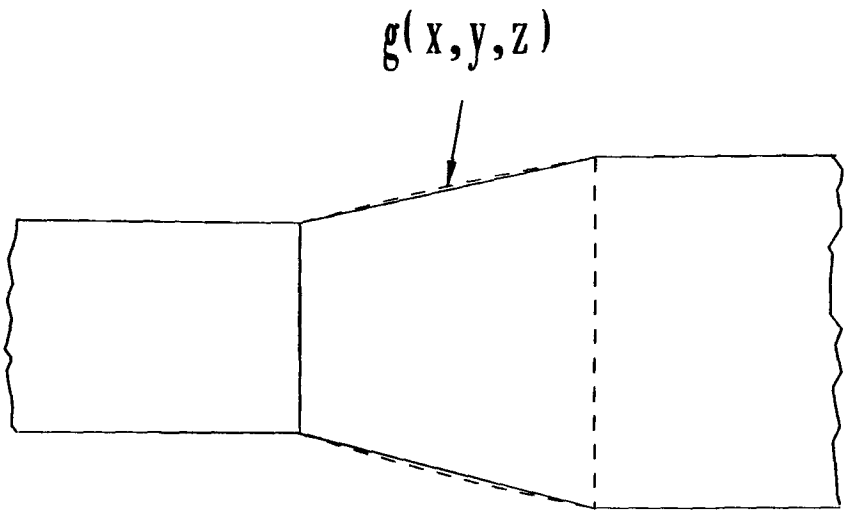

Figure 3.1: Schemetic illustration of the top view of a rectangular bar between the rolls

almost a straight line, and which, in fact, is not unexpected as a result of the requirement for keeping the deformation as uniformly as possible in the roll-pass design, and figure 3.2b and 3.2d, from [17], may serve as a good example amongst many.

However, it seemed that researchers preferred to attempt an exact estimation of the curvature in the calculations with a complicated model. It is imaginable that the contribution of such estimation to the overall value of the energy dissipation would be very small, which leads to the idea that assuming a straight line as the side profile in the present problem is a good approximation. The main purpose of such consideration, of course, is to reduce as much as possible the difficulty in the mathematical handling and the computational demands.

Now, the equation for a straight taper profile, figure 3.3, can be written as the following,

$$y = w(x) = \frac{w_1 - w_0}{l} x + w_0 \tag{3.19}$$

Suppose that $g(x, y, z)$ will assume the form,

$$g(x, y, z) = \frac{qy}{w(x)} = q \tag{3.20}$$

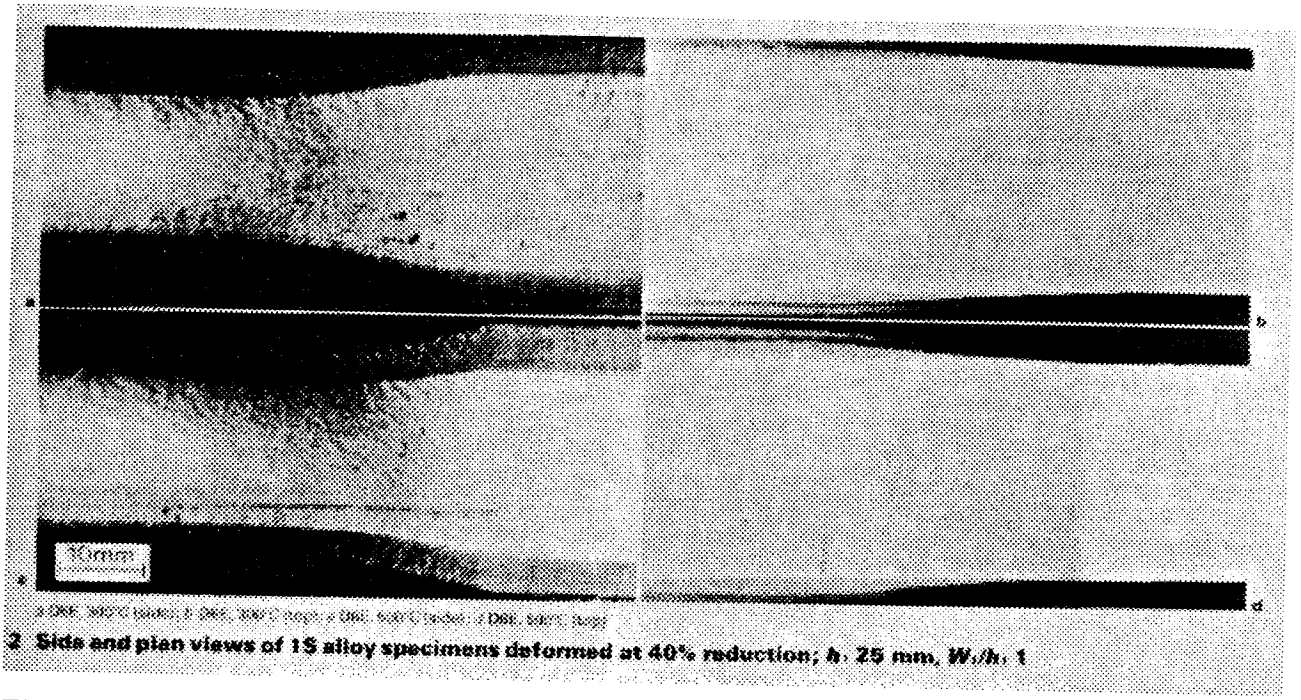

Figure 3.2: Side views(a, c) and plan views(b, d) of 1S alloy specimens deformed at 40% reduction; height: 26 mm, width: 26 mm

where q is some constant, therefore Eq.3.20 meets the constancy restraint of stream surface functional.

Substituting Eq.3.14, Eq.3.18 and Eq.3.20 into Eq.3.3, the following results,

$$q^2 \frac{Q}{tw}\left(\frac{yw'}{w^2} - \frac{yw'}{w^2}\right) = 0 \tag{3.21}$$

which indicates that q can be any constant.

Substituting Eq.3.18 and Eq.3.20 into Eq.3.14, the following are obtained,

$$\begin{aligned} V_x &= -\frac{Qq}{tw} \\ V_y &= -\frac{Qqyw'}{tw^2} \\ V_z &= -\frac{Qqzt'}{wt^2} \end{aligned} \tag{3.22}$$

Through observation, it can be decided that $q = -1$ is the best choice, simply because V_x can never be negative in the current coordinate. Hence, the velocity fields are

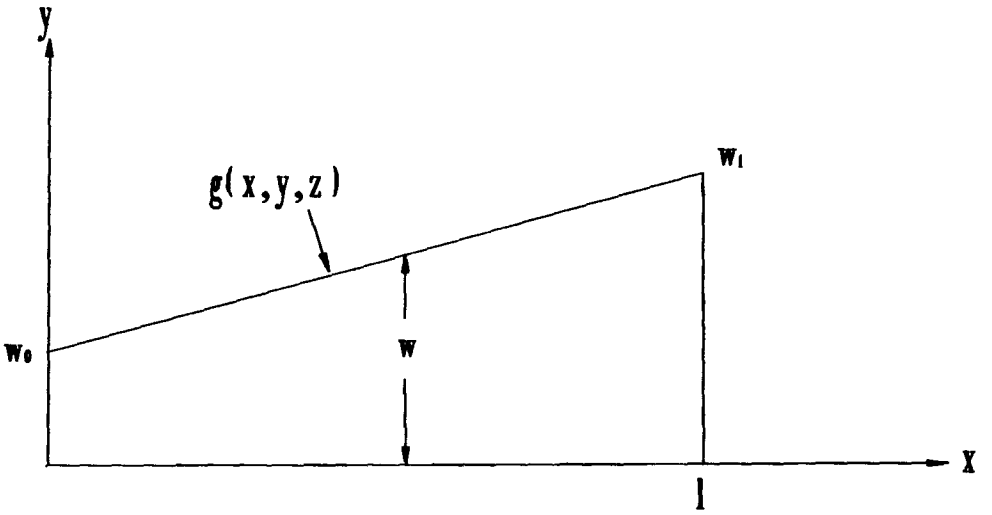

Figure 3.3: The schematic illustration of the simplified side profile of the section between the rolls

determined as

$$\begin{aligned} V_x &= \frac{Q}{tw} \\ V_y &= \frac{Qyw'}{tw^2} \\ V_z &= \frac{Qzt'}{wt^2} \end{aligned} \tag{3.23}$$

3.4 Discussion of the General Solution

At this point, it would be convenient to make a few comments about history. Hill[3] first proposed a similar velocity field solution for the flat rolling and bar drawing in 1963, in which researchers have shown great interests ever since. He must have found a particular way to reach his solution, but, unfortunately, he didn't indicate it[2]. Lahoti, *et al*, considered Hill's work as a "unfinished" one, and continued the work in 1973[4]. However,

[2]For the sake of convenience, Hill's solution is quoted in the following.

"The simplest class of approximating velocity fields with these properties (i.e., the similar assumptions as those of 1, 2 and 5 in Section 2.2, and the same coordinate system, (x,y,z), as in Section 2.3.) has

as Hill himself didn't explain how to relate the solution to the rolling velocity(V_R), neither did Lahoti, *et al.* This, however, becomes significant when a solution to the rolling process, as general as it is in the present work, is sought.

It can be noted from Eq.3.23 that for flat rolling, the following holds,

$$V_0 = V_x|_{x=0} = \frac{Q}{t_0 w_0} \tag{3.25}$$

and this may be rearranged into,

$$Q = V_0 t_0 w_0 \tag{3.26}$$

which indicates an interesting fact that *the constant in the solution is the discharge.*

Accordingly, in the case of

(a) a bar pushed in between two idle rolls,

$$Q = V_0 t_0 w_0 \tag{3.27}$$

where V_0 is a known constant.

(b) a bar pulled through two idle rolls(Steckel rolling, see reference[1]),

$$Q = V_1 t(l) w(l) \tag{3.28}$$

where V_1 is a known constant.

(c) the conventional rolling process,

$$Q = \Theta(x_n, V_R) \tag{3.29}$$

where Θ is some functional. Therefore, in the case of (a) and (b) , there is no need to worry about the estimation of the neutral points. This conclusion is different from the

---

components(here, $h = t$.),

$$v_x = \frac{1}{hw}, \quad v_y = \frac{yw'}{hw^2}, \quad v_z = \frac{zh'}{wh^2} \tag{3.24}$$

within the region bounded by the planes of entry and exit, the faces of the dies, and the lateral surfaces $y = \pm w(x)$, ... Such fields are clearly solenoidal and preserve the configuration; ..... The *immaterial constant of proportionality*(the emphasis is added here) has been chosen so that the total rate of flow across each quarter-section is unity. ....."

one by Oh and Kobayashi[5]. There are some velocity field solutions for the conventional rolling, say, [6], in which the relation, $Q = V_0 t_0 w_0$, was used. This can be considered obscure, because in the conventional rolling, V_0 is an unknown constant before starting the process, besides, V_0 may be temperature dependent.

Thus, it is reasonable and instructive to adopt the prescribed factor Q in the solution, especially when considering the variation of the rolling geometry in the VGR process, where Q may no longer be a constant. In other words, Q may be an instantaneous constant (See next Section).

3.5 Further Considerations

3.5.1 Theoretical Aspect

In the foregoing sections, the solution to the velocity fields has been treated in a general manner. It should have been noted that the derivation of Eq.3.23 is started from the original geometry without any restriction on the motion of the rolls. This is one of the nice things about the solution, as it would be very awkward and unnecessary to construct the component for the up-or-down velocity of rolls at this stage, which could be non-linear. The implication is that when Eq.3.15 is used, which includes a roll-gap function, the variations in the velocity components will naturally be taken into account.

It should also be noted here that in the VGR process, owing to the ever-varying geometry, the velocity vectors in the deformation space become time-dependent, thus, it is a non-steady state process, which is the essential difference from the traditional rolling process, where the geometry is fixed and therefore it is a steady state process. In the present case, however, during the whole process, the geometrical resemblance is basically maintained, which may be the theoretical validity that one set of formulation can be used

in the modelling of the present process. Accordingly, it is both reasonable and necessary to divide the process into a series of small pseudo-steady state deformation steps, that is, by focusing attention on each sampling instant, the geometry may be frozen, then a set of instantaneous solutions can be obtained. And by updating the geometry, a set of approximating numerical solutions may be finally produced, which may serve as a description of the dynamic characters of the process under study. This idea should also be considered as the basis for the discretization procedure in the design of the machine control system.

3.5.2 Technical Aspect

In the VGR process, when the conventional rolling scheme is used, the discharge Q is a variable if the roll peripheral velocity is to be designed as a constant, which, apparently, is preferable; when Steckel rolling scheme is used, if Q were to be designed as a constant, the pulling mechanism would be very complicated. In any case, since Q is preferred to be a variable of the geometry, it is clear that the geometrical parameters have to be determined in advance in order to update Q, which will be a crucial issue in the control scheme.

The roll-gap function G

From machine design standpoint, it is important to consider the feasibility of a simple control scheme at this stage.

In figure 3.4, the two coordinate systems, (x, y, z) and (X, Y, Z), have the following

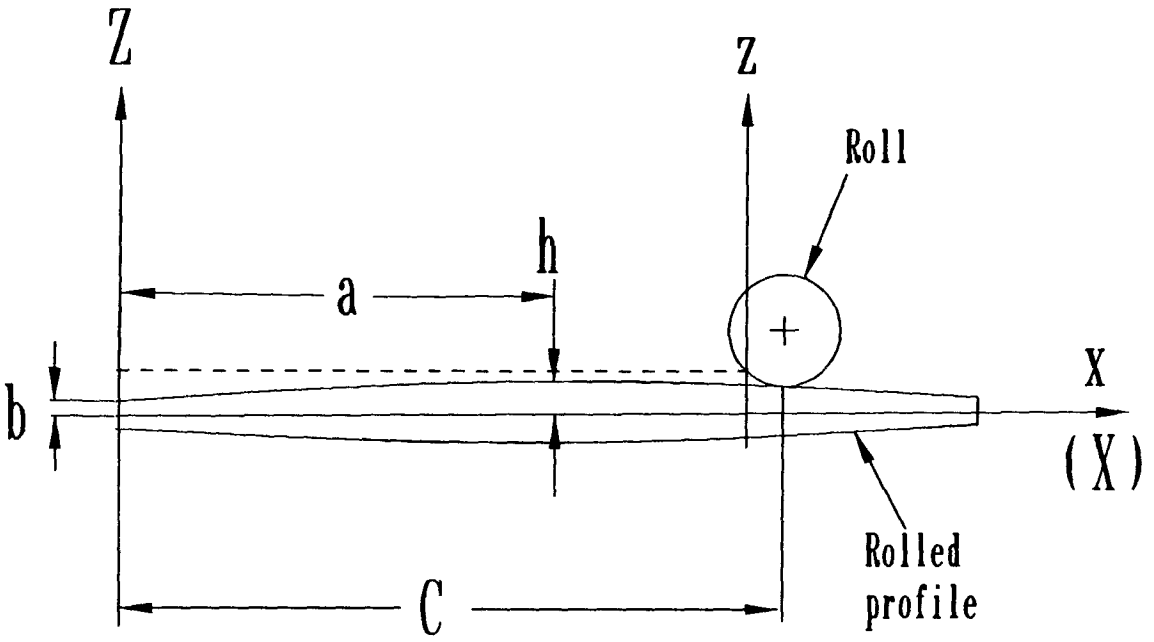

Figure 3.4: The schematic illustration of a parabolic profile in rolling configuration

simple relationship,

$$\left.\begin{aligned} X &= C \\ Z &= z \end{aligned}\right\} \tag{3.30}$$

Here, in order that a typical set of data may be produced, a parabolic type of product has been chosen, although the roll-gap is generically defined.

In coordinates (X, Y, Z), the profile assumes the following form,

$$\left.\begin{aligned} (X-a)^2 &= -2p(Z-h) \\ Z\,|_{x=0} &= b \end{aligned}\right\} \tag{3.31}$$

which can be reduced to

$$(X-a)^2 = -\frac{a^2}{b-h}(Z-h) \tag{3.32}$$

where,

$$a^2 = -2p(b-h) \tag{3.33}$$

i.e.,

$$p = -\frac{a^2}{2(b-h)} \tag{3.34}$$

Let

$$e = \frac{b-h}{a^2} \tag{3.35}$$

then Eq.3.32 becomes

$$Z = e(X-a)^2 + h \tag{3.36}$$

Using Eq.3.30, Eq.3.36 has the following form in coordinates (x, y, z),

$$z = e(C-a)^2 + h \tag{3.37}$$

For notational consistency, Eq.3.37 should be written as

$$G(x+C) = e(C-a)^2 + h \tag{3.38}$$

It can be seen that Eq.3.38 ensures a simple but reliable control scheme. However, detailed discussion is beyond the scope of present work and is left for later; for now, Eq.3.38 is adequate for the present mathematical analysis.

The length of plastic zone

Note that in present problem, the length of the projected arc in contact is also a variable — a function of the roll-gap and t_0, i.e., $l(x)$. From figure 2.3,

$$l(x) = \sqrt{R^2 - [(R-t_0) - G]^2} \tag{3.39}$$

With the above geometrical relationships determined, a new velocity field solution is established, which will be the basis for the next chapter.

Chapter 4

FORMULATION THROUGH UPPER BOUND APPROACH

The upper-bound theorem states that among all kinematically admissible strain rate fields, the actual one minimizes the following expression, using the same notation in [24], p.419,

$$J^* = \int_V \sigma_{ij}^* \dot{\varepsilon}_{ij}^* dV + \sum \int_{S_D} k|\Delta \dot{v}^*| dS_D^* - \int_{S_T} T_i \dot{v}_i^* dS_T \tag{4.1}$$

where, $\dot{\varepsilon}_{ij}^*$ is the strain-rate field derivable from $\dot{v}_i^*$; $\dot{v}_i^*$ is a kinematically admissible velocity field; $|\Delta \dot{v}^*|$ is the amount of velocity discontinuity along the surfaces of discontinuity S_D^*; and σ_{ij}^* satisfies the yield criterion and is associated with $\dot{\varepsilon}_{ij}^*$. In present case, only the conventional rolling scheme is considered, therefore, the back and front tensions are zero, i.e., $T_i = 0$. S_D is the surface where velocity discontinuities occur, and consists of three parts in present problem: the friction surfaces, S_f, between the rolls and the material; the entrance and exit planes, $S_{d0} + S_{d1}$, where shearing occurs; accordingly, $S_D = S_f + S_{d0} + S_{d1}$, Eq.4.1 becomes

$$J^* = \int_V \sigma_{ij}^* \dot{\varepsilon}_{ij}^* dV + \int_{S_f} \tau_0 |\Delta \mathbf{V}_S| dS_f + \int_{S_{d0}+S_{d1}} k|\Delta \mathbf{V}_d| dS_d \tag{4.2}$$

Or using the conventional notations, Eq.4.2 may be written as,

$$J^* = \dot{E}_d + \dot{E}_f + \dot{E}_s \tag{4.3}$$

where,

$$\dot{E}_d = \int_V \sigma_{ij}^* \dot{\varepsilon}_{ij}^* dV \tag{4.4}$$

$$\dot{E}_f = \int_{S_f} mk|\Delta \mathbf{V}_S|dS_f \tag{4.5}$$

$$\dot{E}_s = \int_{S_{d0}+S_{d1}} k|\Delta \mathbf{V}_d|dS_d \tag{4.6}$$

Definitions of various terms in Eqn.4.4 through 4.6 is given in the following sections.

4.1 The Strain Rates

The six strain tensors are defined as the following,

$$\begin{aligned} \dot{\varepsilon}_x &= \frac{\partial V_x}{\partial x} \quad \dot{\varepsilon}_{xy} = \frac{1}{2}(\frac{\partial V_y}{\partial x} + \frac{\partial V_x}{\partial y}) \\ \dot{\varepsilon}_y &= \frac{\partial V_y}{\partial y} \quad \dot{\varepsilon}_{yz} = \frac{1}{2}(\frac{\partial V_y}{\partial z} + \frac{\partial V_z}{\partial y}) \\ \dot{\varepsilon}_z &= \frac{\partial V_z}{\partial z} \quad \dot{\varepsilon}_{zx} = \frac{1}{2}(\frac{\partial V_x}{\partial z} + \frac{\partial V_z}{\partial x}) \end{aligned} \tag{4.7}$$

Substituting Eq.3.23 into Eq.4.7 and re-arranging it, the following results,

$$\begin{aligned} \dot{\varepsilon}_x &= -Q\frac{1}{tw}(\frac{t'}{t} + \frac{w'}{w}) \\ \dot{\varepsilon}_y &= Q\frac{w'}{tw^2} \\ \dot{\varepsilon}_z &= Q\frac{t'}{wt^2} \\ \dot{\varepsilon}_{xy} &= -\frac{Q}{2}\frac{yw'}{tw^2}(\frac{t'}{t} + \frac{2w'}{w}) \\ \dot{\varepsilon}_{zx} &= \frac{Q}{2}\frac{z}{wt^2}[t'' - t'(\frac{2t'}{t} + \frac{w'}{w})] \\ \dot{\varepsilon}_{yz} &= 0 \end{aligned} \tag{4.8}$$

4.2 The Energy Rates

4.2.1 The energy dissipation rate due to deformation($\dot{E}_d$)

Using the Lévy-Mises equations, Eq.4.4 may be written as,

$$\dot{E}_d = \frac{2}{\sqrt{3}}\sigma \int_V \sqrt{\frac{1}{2}\dot{\varepsilon}_{ij}\dot{\varepsilon}_{ij}}dV \tag{4.9}$$

Since,

$$\begin{aligned}\frac{1}{2}\dot{\varepsilon}_{ij}\dot{\varepsilon}_{ij} &= \frac{1}{2}(\dot{\varepsilon}_x^2 + \dot{\varepsilon}_y^2 + \dot{\varepsilon}_z^2) + \dot{\varepsilon}_{xy}^2 + \dot{\varepsilon}_{zx}^2 + \dot{\varepsilon}_{yz}^2 \\ &= \frac{1}{2}\frac{Q^2}{t^2w^2}(I^2 + M^2y^2 + N^2z^2)\end{aligned} \tag{4.10}$$

where,

$$\begin{aligned}I &= \sqrt{2\left[\left(\frac{w'}{w}\right)^2 + \left(\frac{t'}{t}\right)^2 + \frac{t'w'}{tw}\right]} \\ M &= \sqrt{\frac{1}{2}}\frac{w'}{w}\left(\frac{t'}{t} + \frac{2w'}{w}\right) \\ N &= \sqrt{\frac{1}{2}}\left|\frac{t''}{t} - \frac{t'}{t}\left(\frac{2t'}{t} + \frac{w'}{w}\right)\right|\end{aligned} \tag{4.11}$$

Substitution of Eq.4.10 into Eq.4.9 results the following,

$$\dot{E}_d = 4\sigma \int_0^l \int_0^t \int_0^w \sqrt{\frac{2}{3}}\frac{Q}{tw}\sqrt{I^2 + M^2y^2 + N^2z^2}dydzdx \tag{4.12}$$

After integration against y and z, Eq.4.12 becomes

$$\dot{E}_d = \sqrt{\frac{2}{3}}Q\sigma \int_0^l Z(x)dx \tag{4.13}$$

where,

$$\begin{aligned}Z(x) &= \sqrt{I^2 + M^2y^2 + N^2z^2} + \frac{I^2 + M^2w^2}{Nt}\ln\frac{Nt + \sqrt{I^2 + M^2w^2 + N^2t^2}}{\sqrt{I^2 + M^2w^2}} \\ &+ \frac{2I^2}{MNtw}\left[P_1(\sqrt{I^2 + M^2w^2}, Mw, Nt) - P_1(I, 0, Nt)\right] \\ &+ \frac{2}{MNtw}\left[P_1(\sqrt{I^2 + M^2w^2}, Mw, Nt) - P_1(I, 0, Nt)\right]\end{aligned} \tag{4.14}$$

where,

$$\begin{aligned} P_1(a,b,c) &= \int_0^c \ln(b+\sqrt{a^2+x^2})dx \\ &= c\ln(b+\sqrt{a^2+c^2}) - c + b\ln\frac{(\sqrt{a^2+c^2}+c)}{a} \\ &\quad +2\sqrt{a^2-b^2}\tan^{-1}\left[\frac{\sqrt{a^2-b^2}}{a+b}\frac{(\sqrt{a^2+c^2}-a)}{c}\right] \end{aligned} \tag{4.15}$$

$$\begin{aligned} P_2(a,b,c) &= \int_0^c x^2\ln(b+\sqrt{a^2+x^2})dx \\ &= \frac{1}{3}\left[c^3\ln(b+\sqrt{a^2+c^2}) - \frac{1}{3}c^3 + c(a^2-b^2)\right. \\ &\quad +\frac{1}{2}bc\sqrt{a^2+c^2} - \frac{1}{2}b(3a^2-2b^2)\ln\frac{(\sqrt{a^2+c^2}+c)}{a} \\ &\quad \left.-2(a^2-b^2)^{\frac{3}{2}}\tan^{-1}\left(\frac{\sqrt{a^2-b^2}}{a+b}\frac{(\sqrt{a^2+c^2}-a)}{c}\right)\right] \end{aligned} \tag{4.16}$$

4.2.2 The energy dissipation rate due to friction between roll surfaces and workpiece($\dot{E}_f$)

From figure 4.1, the velocity discontinuity between the surfaces of roll and material can be expressed as the following,

$$\Delta\mathbf{V}_S = \mathbf{V}_y + \mathbf{V}_R - (\mathbf{V}_x + \mathbf{V}_z) \tag{4.17}$$

and the magnitude,

$$\begin{aligned} |\Delta\mathbf{V}_S| &= \sqrt{V_y^2 + (V_R - \sqrt{V_x^2+V_z^2})^2} \\ &= Q\sqrt{\left(\frac{yw'}{tw^2}\right)^2 + \left(\frac{V_R}{Q} - \frac{\sqrt{1+t'^2}}{wt}\right)^2} \end{aligned} \tag{4.18}$$

Note that on the surface, $z = t(x)$. Then Eq.4.5 becomes,

$$\dot{E}_f = 4mkQ\int_0^l\int_0^w \sqrt{\left[\left(\frac{yw'}{tw^2}\right)^2 + \left(\frac{V_R}{Q} - \frac{\sqrt{1+t'^2}}{wt}\right)^2\right](1+t'^2)}dxdy \tag{4.19}$$

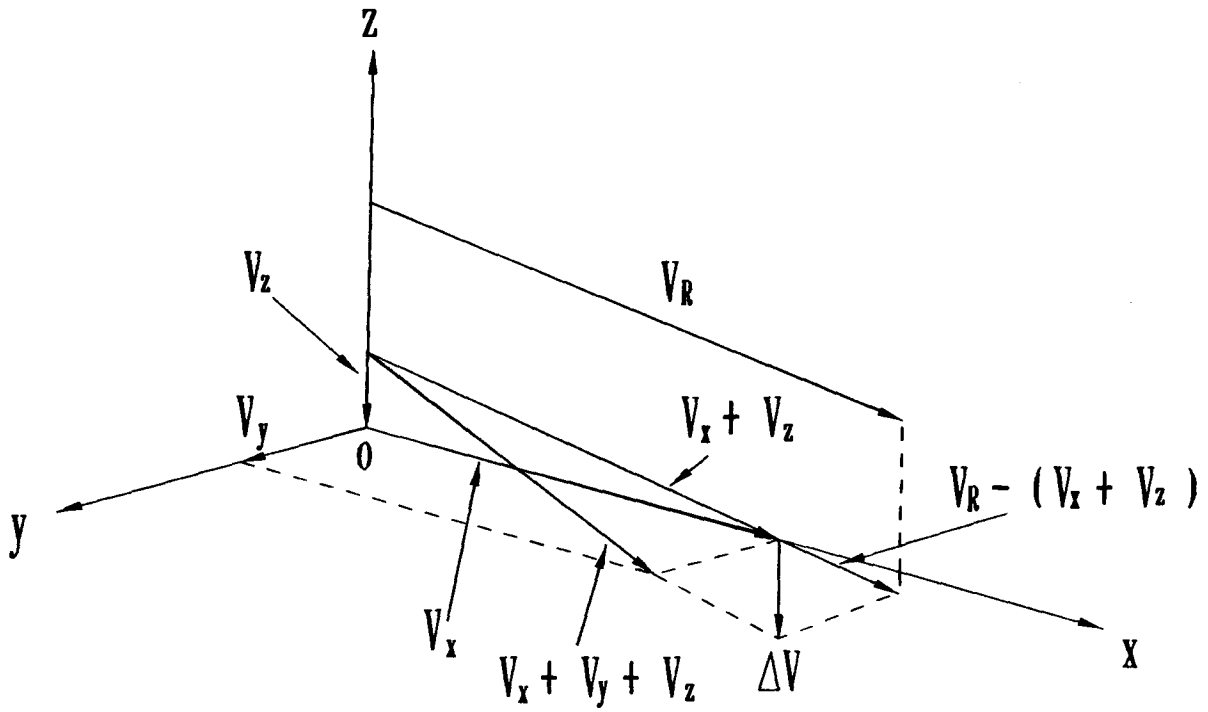

Figure 4.1: The schematic illustration of the velocity vector space in conventional rolling process

and after integration against y and z, Eq.4.19 becomes

$$\dot{E}_f = 2mkQ \int_0^l F(x)\sqrt{1+t'^2}dx \tag{4.20}$$

where,

$$F(x) = \frac{w}{2}\left\{\sqrt{\left(\frac{w'}{tw}\right)^2 + \left(\frac{V_R}{Q} - \frac{\sqrt{1+t'^2}}{wt}\right)^2} + \frac{wt}{w'}\left(\frac{V_R}{Q} - \frac{\sqrt{1+t'^2}}{wt}\right)^2 \cdot \ln\left[\left\{\frac{w'}{wt} + \sqrt{\left(\frac{w'}{tw}\right)^2 + \left(\frac{V_R}{Q} - \frac{\sqrt{1+t'^2}}{wt}\right)^2}\right\} \div \left|\frac{V_R}{Q} - \frac{\sqrt{1+t'^2}}{wt}\right|\right]\right\} \tag{4.21}$$

4.2.3 The energy dissipation rate due to velocity discontinuities ($\dot{E}_s$)

From figure 4.1, at the entrance plane,

$$\Delta \mathbf{V}_{d0} = \mathbf{V} - \mathbf{V}_x = \mathbf{V}_y + \mathbf{V}_z \tag{4.22}$$

and the magnitude,

$$|\Delta \mathbf{V}_{d0}| = \sqrt{V_y^2 + V_z^2} \tag{4.23}$$

And at the exit plane, since the width of the deforming body is almost the same as the width of the rigid body, we may assume $\mathbf{V}_y = 0$; thus, from figure 4.1, the following holds,

$$\Delta \mathbf{V}_{d1} = \mathbf{V} - \mathbf{V}_x = \mathbf{V}_y = \mathbf{0} \tag{4.24}$$

Substitution of Eq.4.23 and Eq.4.24 into Eq.4.6 gives, note that, $V_0 = Q/w_0 t_0$,

$$\begin{aligned} \dot{E}_s &= 4k \int_{S_{d0}} \sqrt{(V_y^2 + V_z^2)_{x=0}} dS_d \\ &= 4kV_0 \int_0^{w_0} \int_0^{t_0} \sqrt{\left(\frac{yw'}{w}\right)^2_{x=0} + \left(\frac{zt'}{t}\right)^2_{x=0}} dzdy \end{aligned} \tag{4.25}$$

The integration of Eq.4.25 results in the following,

$$\dot{E}_s = kQS(x, w_1) \tag{4.26}$$

where,

$$\begin{aligned} S(x, w_1) = &\left[\sqrt{t'^2 + w'^2} + \frac{t'^2}{w'} \ln \frac{w' + \sqrt{t'^2 + w'^2}}{|t'|} + \right. \\ &\left. \frac{4}{t'w'} P_2(t', t', w') - \frac{2}{3}\frac{w'^2}{t'}(\ln w' - \frac{1}{3})\right]_{x=0} \end{aligned} \tag{4.27}$$

4.3 The Minimization Procedure

Since the unknown parameters in the velocity fields solution are w_1 and x_n, the problem is reduced to solving the following non-linear equations,

$$\frac{\partial J^*}{\partial w_1} = 0, \qquad \frac{\partial J^*}{\partial x_n} = 0 \tag{4.28}$$

By substituting Eq.4.3 into Eq.4.28, the equations to be minimized are obtained,

$$\frac{\partial \dot{E}_d}{\partial w_1} + \frac{\partial \dot{E}_f}{\partial w_1} + \frac{\partial \dot{E}_s}{\partial w_1} = 0 \tag{4.29}$$

$$\frac{\partial \dot{E}_d}{\partial x_n} + \frac{\partial \dot{E}_f}{\partial x_n} + \frac{\partial \dot{E}_s}{\partial x_n} = 0 \tag{4.30}$$

4.3.1 The derivatives of the geometry

From Eq.3.19, the following is obtained,

$$w' = (w_1 - w_0)\frac{1}{l} \tag{4.31}$$

along with

$$\frac{\partial w}{\partial w_1} = \frac{x}{l} \tag{4.32}$$

and

$$\frac{\partial w'}{\partial w_1} = \frac{1}{l} \tag{4.33}$$

through which the following results readily,

$$\left(\frac{\partial w'}{\partial w_1}\right)_{x=0} = \frac{1}{l} \tag{4.34}$$

and Eq.4.31 also gives the following,

$$w_0' = (w_1 - w_0)\frac{1}{l} \tag{4.35}$$

4.3.2 The neutral point

Apparently, in present case, the neutral point is ever-changing. However, the following still holds instantaneously for each frozen moment, figure 4.1,

$$\mathbf{V}_R = \mathbf{V}_x(x_n) + \mathbf{V}_z(x_n) \tag{4.36}$$

Using Eq.3.23 and note that, $z = t(x_n)$, we have the following,

$$V_R = \frac{Q}{wt}\sqrt{1+t'}\Big|_{x=x_n} \tag{4.37}$$

or it may be written as,

$$\frac{V_R}{Q} = \frac{\sqrt{1+t'(x_n)}}{w(x_n)t(x_n)} \tag{4.38}$$

or,

$$Q(x_n) = V_R \frac{w(x_n)t(x_n)}{\sqrt{1+t'(x_n)}} \tag{4.39}$$

4.3.3 Solutions

The analytical solution to Eqn.4.28 is too complicated and may be found in Appendix A.

The numerical solution is obtained by coding in MATLAB. A CPU time of 15 seconds for each cycle of calculation is achievable on Sparc-I SUN workstation. The results are given in Chapter 6.

Chapter 5

FLOW STRESS MODEL

In the foregoing chapters, a fundamental geometric description of the process has been given. To achieve a reasonable control of the roll-gap in the VGR process, a detailed and accurate roll force change prediction is required. It should also be noted that, in order that the newest developments in material science may be adopted in the calculation, the assumption that the materials are rigid-perfectly plastic is in need of further modification. In other words, it is necessary to establish a correlation describing the changes in flow stress as the workpiece moves through the rolls and between the passes, so the changes in rolling forces may be predicted. An adequate mathematical model of flow stress incorporating the thermal characteristics of materials would be of great importance in implementing the VGR process and in controlling the final properties of the rolled products.

5.1 Dynamic Flow Stress

Unlike cold working, the hot deformation of steels at elevated temperatures (above the recrystalization temperature) may be divided into three transient stages[25][26][27] —

1. Microstrain deformation. This is the interval during which the plastic strain rate increases from zero to the approximate forming rate, and the stress in the workpiece rises rapidly, Fig. 5.1. The loading slopes are rate controlling in this interval.

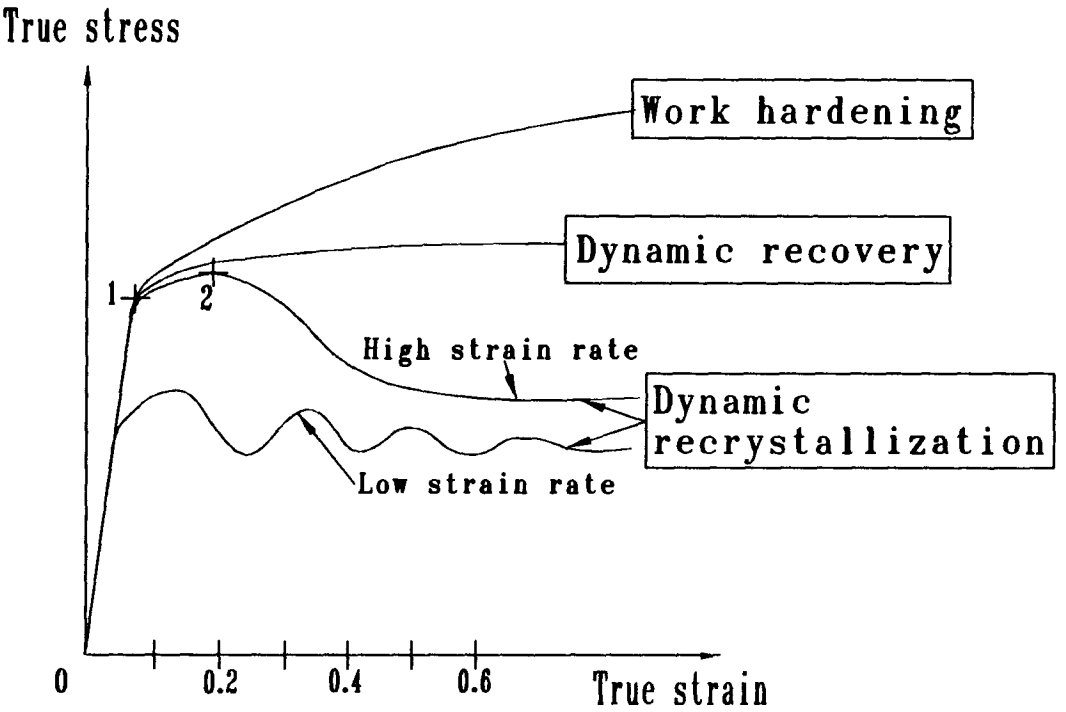

Figure 5.1: Schematic flow curve for metals at elevated temperature. From point 0 to 1, the plastic strain rates increase rapidly. Note that the scale for the strain is arbitrarily chosen from typical C-Mn steels[27] to illustrate a possible range in applications

2. Plastic yielding. The region of the yield stress marks the beginning of work hardening. The slope is temperature and rate sensitive, but in general, is gradually decreasing.

3. Dynamic restoration. This stage is most complicated due to the concurrent operations of the strain hardening and softening. Generally speaking, if the strain rate is low and the hardening effect is only offset by the dynamic recovery process alone, a steady state will quickly be reached, so a simple flow curve results.

   The alternative restoration process is dynamic recrystallization, which modifies the flow curve in the following ways. At high strain rates, the flow stress rises to a maximum at peak strain(point 2 in figure 5.1), and then it diminishes to a value intermediate between the yield stress and the peak stress(See figures in Appendix

B). At low strain rates, the dynamic recrystallization process causes a softening followed by a oscillatory type of flow curve before a steady state is reached, figure 5.1.

In [27], I. Tamura, et al, stated the following.

> For most commercial steels, dynamic recovery behaviour is observed in iron and carbon steel deformed in the ferritic region, or in ferritic alloy steels such as silicon iron. Dynamic recrystallization takes place in the hot-deformation of γ including HSLA steels and austenitic alloy steels.

This may serve as a general guideline, although care should be taken for each different material.

The reduction ratio in the VGR process can be anything between 8% and 50%, which corresponds to the true strain range from 0.051 to 0.693. From figure 5.1, it is clear that the flow stress will vary significantly during each pass. In other words, in reality, the materials are rate dependent within the strain range of hot rolling. Accordingly, instead of using a flow stress value corresponding to the steady state, which itself may result in conflicts, it is necessary to have a flow stress model to count in such variations.

5.2 Incorporation of Rate Dependency

It has long been concluded that the flow stress model that gives a complete description of the hot deformation of steels in the roll-bite assumes the form[28]:

$$\sigma = f(\textit{composition of the alloying elements}, T, \varepsilon, \dot{\varepsilon}) \tag{5.1}$$

where T is temperature.

As is stated in Section 3.5, the VGR process is a nonsteady state forming process, and in the last Section we concluded that it is not reasonable to use a constant yield stress

throughout the whole process. A yield function similar to the above form would be very important in obtaining a solution close to reality. Therefore, modifications are needed since, theoretically, the upper bound approach is only valid in rigid perfectly plastic materials. It is clear that, unless the strain is beyond the steady state point, which is not the case in rolling process, the state of rigid-perfectly plastic deformation will never be reached. In order that rate dependent[1] effects can be incorporated, the concept of instantaneous yield conditions has to be adopted and further assumptions must be made.

First of all, it is interesting to note that the available flow stress data are usually obtained from three sources: (1) uniaxial compression tests; (2) thin-walled tortion tests; (3) plain strain compression tests. A close examine of those tests tells one that it is impossible to get rid of the rate effects. Therefore, the results from these tests are usually similar to those in figure 5.1. Figures B.1—B.4 in Appendix B give some results from experiments that clearly show irregularities in flow stress due to the restoration process. This indicates that even though a perfectly plastic material is assumed, flow stress value at the steady state can not be used. Instead, one has to use the data at certain strain points. The implication is that the solution calculated from the available experimental yield stress data can only be an approximation. Nevertheless, this is the usual practice in modelling of the conventional rolling process.

Then, the usual assumption that the material is perfectly plastic may be modified, that is, the appropriate assumption in the real situation may be that the material has a isotropic rate dependency[2]. Thus, the material is still a Mises material, and the yield locii become a set of uniform expansions of the previous one, i.e., a set of circular cylinders.

Furthermore, a similar assumption adopted by Hill[17], when an extrusion process was considered, should also be made. That is, the mean strain of the deforming body remains

[1]The definition for rate dependency may be given differently by different authors. In this work, the term, "rate", should include the temperature decreasing rate, the rate of restoration and the strain rate.

[2]The condition of isothermal is implied.

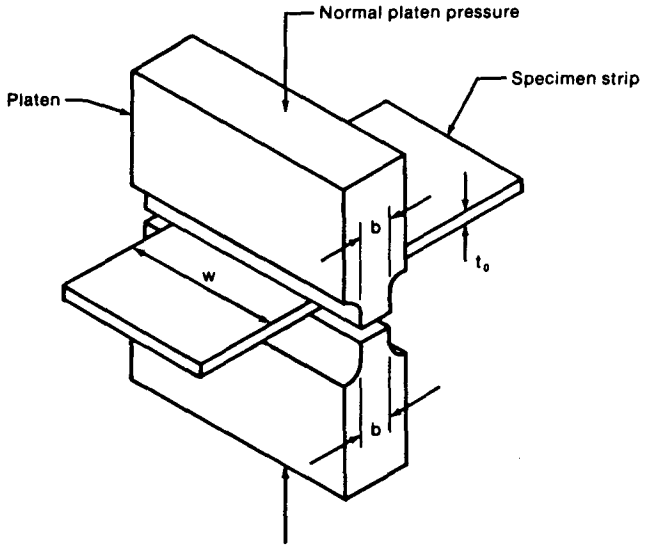

Figure 5.2: Schematic setting of plane compression test

unchanged regardless of the rate dependent characteristics of the workpiece material. This implies that the mean strain of such a rate dependent material is the same as that of a perfectly plastic material, since isotropy and volume constancy are assumed. Based upon this assumption, the concept of mean equivalent strain, or effective strain, $\bar{\varepsilon}$, and of mean strain rate can be introduced.

5.3 Mean Values of Strain and Strain Rate

In Eqn.5.1, it should be clear that for a practical purpose, σ, ε, $\dot{\varepsilon}$, and T can only be given in mean values.

5.3.1 Mean Strain

To explain the concept of mean equivalent strain, it is helpful to look at the approach applied in the plane compression test. In figure 5.2, the lateral strain may be taken as zero, i.e., $\varepsilon_x = 0$, and volume constancy is assumed. The thickness strain ε_z is

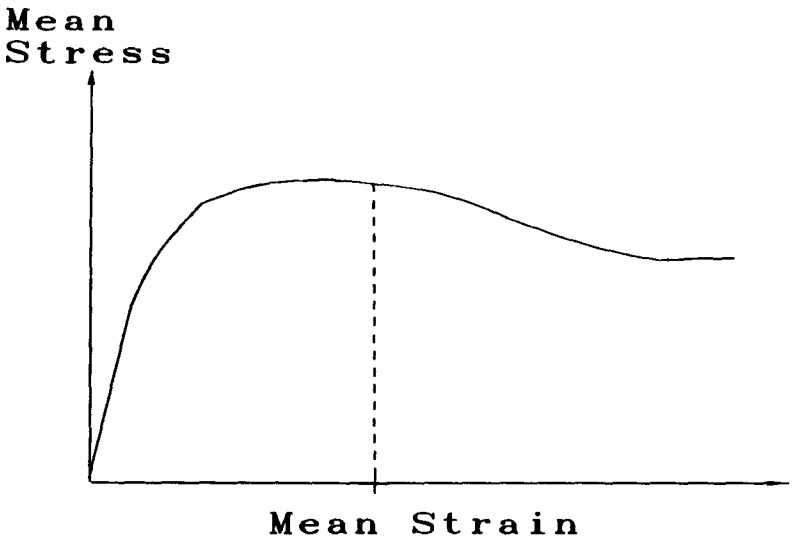

Figure 5.3: Schematic relation between mean yield stress and mean equivalent strain in plane compression test

numerically equal to longitudinal strain ε_y. These results may then be used in the Lévy-Mises relationship,

$$\begin{aligned} \bar{\varepsilon} &= \frac{1}{3}\sqrt{2[(\varepsilon_x - \varepsilon_y)^2 + (\varepsilon_y - \varepsilon_z)^2 + (\varepsilon_z - \varepsilon_x)^2]} \\ &= \frac{2}{\sqrt{3}}\varepsilon_z \end{aligned} \tag{5.2}$$

which indicates that the mean equivalent strain is proportional to the strain in the direction of reduction. So the mean flow stress σ_m in such tests is usually given as

$$\sigma_m = F_1(\varepsilon_z) = F(\bar{\varepsilon}) \tag{5.3}$$

where F is determined by the test. The results would be similar to those in figure 5.3.

The above approach reveals an important idea. For an isotropic rate dependent material, the mean yield stress may be obtained by establishing first an appropriate procedure to calculate mean equivalent strain. This idea was successfully used by many researchers in the past, such as, Kudo[29][30], when upper bound approach was applied. Johnson[31] and Dodeja and Johnson[32] used it in an analysis of forging and extrusion process in an upper bound solution, where the $\bar{\varepsilon}$ was calculated through the estimation of the total power consumed while assuming the workpiece is perfectly plastic.

For the present case, since no bulge is assumed, the following method described in [33][34] can be used in estimating the mean strain,

$$\bar{\varepsilon} = \frac{1}{l}\int_0^l \sqrt{\varepsilon_x^2 + \varepsilon_y^2 + \varepsilon_z^2}\, dx \tag{5.4}$$

where the components, ε_x, ε_y and ε_z are taken as the principle strains.

The assumptions in Section 2.2 imply proportional straining, i.e.,

$$\varepsilon_x + \varepsilon_y + \varepsilon_z = 0 \tag{5.5}$$

which leads to

$$\bar{\varepsilon} = \frac{1}{l}\int_0^l \sqrt{\varepsilon_y^2 + \varepsilon_y\varepsilon_z + \varepsilon_z^2}\, dx \tag{5.6}$$

where the instantaneous strains are usually defined as,

$$\varepsilon_z = \ln\frac{t(x)}{t_0} \qquad \varepsilon_y = \ln\frac{w(x)}{w_0} \tag{5.7}$$

Note that sometimes the stress-strain tests were carried out in uniaxial compression. Then, the following conversion should be done before using the results from Eqn.5.4,

$$\bar{\varepsilon}_u = \frac{2}{\sqrt{3}}\bar{\varepsilon} \tag{5.8}$$

It is noticed in the literature that the stress testing data for rolling process were traditionally arranged in a correlation between stress and reduction ratio, which is convenient in application. In such cases, a mean reduction ratio may be calculated first as follows,

$$r_m = 1 - e^{\bar{\varepsilon}} \quad \text{or} \quad r_{mu} = 1 - e^{\bar{\varepsilon}_u} \tag{5.9}$$

5.3.2 Mean Strain Rate

In the present work, a similar hypothesis in calculating the mean strain described by Chakrabarty[35] will be used, which is the following.

Considering the second invariant of the plastic strain increment tensor, an equivalent plastic strain increment is defined as

$$\dot{\bar{\varepsilon}} = \sqrt{\frac{2}{3}\dot{\varepsilon}_{ij}\dot{\varepsilon}_{ij}} \tag{5.10}$$

Therefore,

$$\dot{\bar{\varepsilon}}_m = \frac{1}{V}\int_V \dot{\bar{\varepsilon}}\, dV \tag{5.11}$$

By substituting Eqn.5.11 into Eqn.5.3, a rate dependent hypothesis, which is exactly the same as the strain-hardening hypothesis described in [35], may be introduced as the following,

$$\sigma_m = F(\dot{\bar{\varepsilon}}_m) \tag{5.12}$$

where F should also be considered as a function of the other two variables(the mean strain and the mean temperature). Accordingly, the strain rate increments may be calculated by firstly assuming that the material is a perfectly plastic, so Eqn.4.3 can be used to obtain a reasonable mean strain.

5.4 Temperature Prediction

Although it is known that temperature has a dominant effect on the magnitude of the flow stress, not many models incorporating temperature changes have been formulated for the purpose of predicting the flow stress[36]. A large amount of research work on the thermal effects has been done in the past two decades. An excellent review may be found in reference [37].

5.4.1 Basic Considerations

Since the VGR process is designed for the rolling of rather small workpieces, the temperature of such small workpiece will drop very quickly. Accordingly, drastic changes in flow stress during rolling will be expected.

The important variables that have great influence on temperature changes are:

- Processing time per pass.
- Interpass time.
- Temperature of the rolls (determined by cooling methods).
- Conditions of the roll-workpiece interface.

It is clear that the VGR process planning will largely depend on the above variables. A valid correlation is needed.

The present work is based on the idea that a combination of separate submodels, such as, deformation, flow stress and force, etc., should be used, so that new developments can be easily adopted. Fundamental analysis is preferred, since all the empirical formulae were meant for large mill operations and are difficult to make necessary changes.

All the available fundamental analyses, e.g., [37][38][39], are similar in that a heat transmission from the furnace to the finish stands was considered. In the present case, a relatively small machine is considered, and the temperature will drop due to contacting the rolls and the run-out table, convection to the spray and the air, and radiation.

It is conceivable that in such a heat transfer chain, the temperature distribution of the rolls is affected by too many factors, such as the cooling method, the size and structure, the surface condition and the number of rolls, etc. It is almost impossible to give a accurate prediction due to the variation of the interface area, even if one has a detailed specifications of the process. Therefore, the present author believes that, when the VGR process is considered, the temperature of the rolls has to be obtained from some sensor reading.

5.4.2 Heat Conduction Model

The heat conduction in a isotropic solid, the rectangular bar being rolled, may be modelled by the following equation:

$$k_s\left(\frac{\partial^2 T}{\partial x^2}+\frac{\partial^2 T}{\partial y^2}+\frac{\partial^2 T}{\partial z^2}\right)+\dot{q}=\rho_w C_w\frac{\partial T}{\partial \tau} \tag{5.13}$$

The coordinates are the same as before. The present work will only consider one dimensional transient heat transfer, and necessary simplifications to Eqn.5.13 have to be made.

5.4.3 Assumptions

1. In order to simplify the calculation in the temperature model, it is assumed that the workpiece is always a rectangular bar when convection and radiation are considered, that is to say that the influence on heat transfer due to the changes in the geometry is ignored. Mean values of the dimensions will be used in calculation.

2. Heat conduction along the length of the product is negligible in comparison with the heat transfer by the movement of the product.

3. The temperature gradients in the roll-gap along the width direction is negligible since no contact is made between the sides and the rolls. In the roll-bite, only one-dimensional transfer will be considered. It is assumed that the small amount[3] of heat generated by the deformation, and of heat generated by friction between the rolls and the workpiece will somewhat offset the heat loss from the two open sides in the roll-bite.

[3]It can be easily found out that the heat generated by deformation in the roll-bite is very small. Some researchers, say, [41], calculated the amount of temperature raised due to deformation in plate and strip rolling and the result is only about 20 °C. The contribution of such a variation in temperature to the change in flow stress is negligible.

Then, it may be assumed that $\dot{q} = 0$. Thus, Eqn.5.13 is reduced to:

$$k_s \frac{\partial^2 T}{\partial z^2} = \rho_w C_w \frac{\partial T}{\partial \tau} \tag{5.14}$$

4. The temperature gradient at the centerplane through the thickness is assumed as zero. Previous work[40] showed that no temperature difference exists between the top and bottom surfaces of the workpiece. This indicates that no heat flows across the centerplane. That is,

$$\frac{\partial T(0,\tau)}{\partial z} = 0 \tag{5.15}$$

5. The effect of the scale layer on the surfaces of the workpiece can be ignored. This is a usual practice in the research works, due to the lacking of experimental data.

6. It is assumed that the stages of cooling under consideration are: radiation and convection before entry, cooling by contacts to the rolls, radiation and convection after exit. The effect of contacting to the entry and exit tables is ignored, because no suitable data can be applied. Besides, when the workpiece is out of the roll-bite, the body temperature gradient is ignored, only surface temperature will be considered.

7. Thermal conductivities, k_s, and specific heat, C_p, of steels with various carbon contents as function of temperature was established by Devadas[37] by fitting available data from BISRA Tables[42]. The results are shown in figures 5.4 and 5.5. These two figures indicate that, with the temperature increasing to about 1200 °C, the effect of varying the carbon contents on k_s and C_p decreases. In cases of 0.4 C and 0.8 C, the differences are negligible.

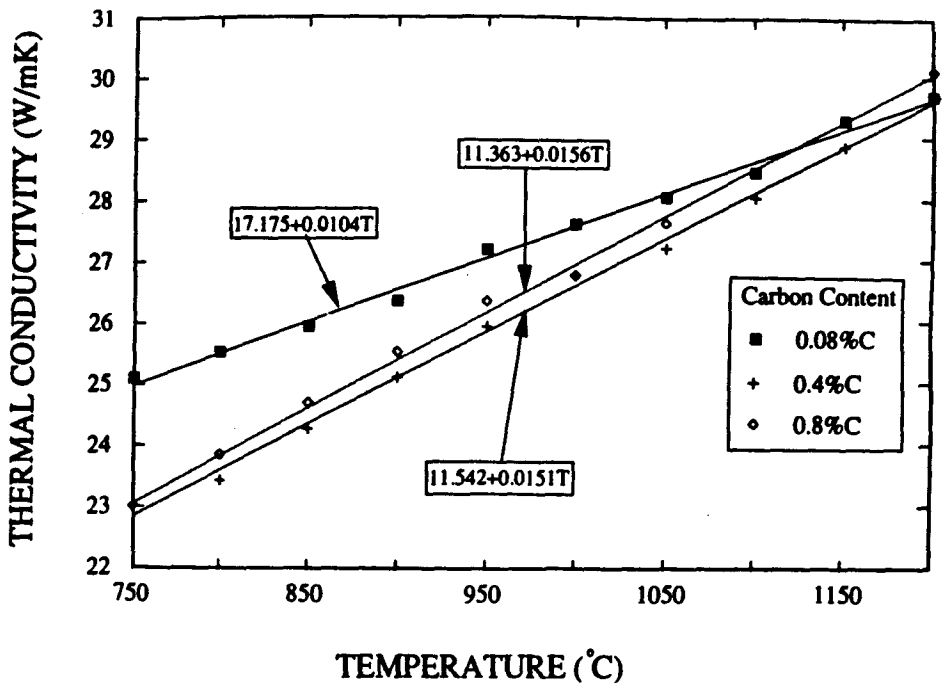

Figure 5.4: Thermal conductivity as a function of temperature for 3 carbon content 0.08 C, 0.4 C, 0.8 C in austenite phase. (From Devadas, 1989)

Figure 5.6 and 5.7 show the results from fitting some data in [43] for two different C-Mn steels. When choosing the appropriate functions for thermal conductivity and specific heat, reference may be made to these results:

$$C_w = -1.11024(10^{-4})T^2 + 0.3670T + 399.5600 \quad \text{(for 0.19C 1.39Mn steel)} \tag{5.16}$$

$$C_w = 0.2511T + 411.4217 \quad \text{(for 0.37C 1.44Mn steel)} \tag{5.17}$$

$$C_w = -0.0001T^2 + 0.4103T + 390.9195 \quad \text{(for 0.23C 1.51Mn steel)} \tag{5.18}$$

$$k_s = -0.0246T + 49.202 \quad \text{(for all C} > 0.15 \text{ C} - \text{Mn steels)} \tag{5.19}$$

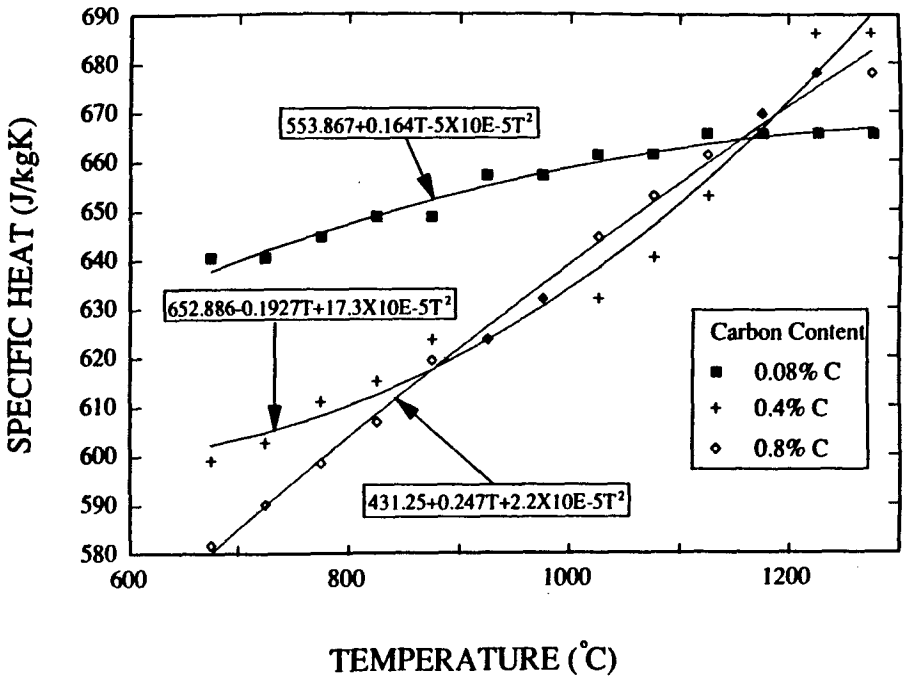

Figure 5.5: Specific heat as a function of temperature for 3 carbon content 0.08 C, 0.4 C, 0.8 C in austenite phase. (From Devadas, 1989)

5.4.4 Initial and Boundary Conditions

The initial temperature of the workpiece is taken as that when it is moved out of the furnace. i.e.,

$$T(z,0) = T_0 \tag{5.20}$$

In addition to Eqn.5.15, Eqn.5.14 is subjected to the following conditions, which can be derived from heat balance.

Owing to symmetric cooling, at the interfaces between roll and workpiece, only consider convection, we have the following,

$$-k_s \frac{\partial T}{\partial z}\bigg|_{z=t(x)} = H(\tau)[T(t,\tau) - T_r] \tag{5.21}$$

where $H(\tau)$ is the heat transfer coefficient, to which further definition is given in Section 5.4.6.

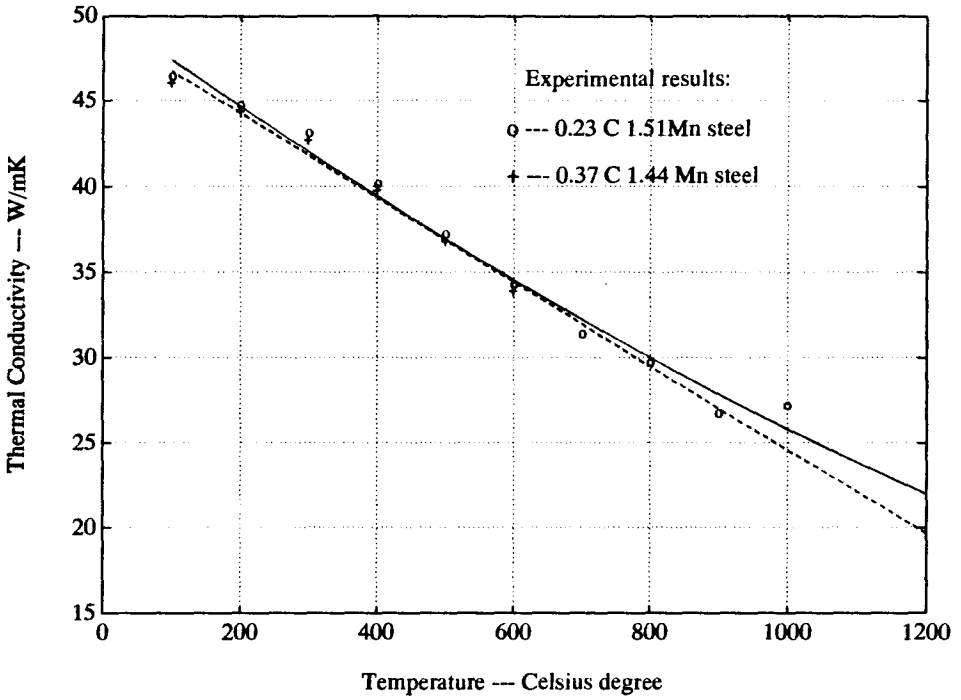

Figure 5.6: Thermal conductivity as a function of temperature for C-Mn steels

5.4.5 Solution to the Heat Conduction Equation

In terms of computing speed, it is preferred to have an analytical solution to Eqn.5.15. The following is a brief account of the method used for finding the solution. A detailed description may be found in [51].

1. Assuming the solution has two parts — one is steady and the other is transient,

$$T(z,\tau) = U(z) + v(z,\tau) \tag{5.22}$$

then, using the boundary conditions, the steady part, $U(z)$, may be determined as

$$U(z) = T_r \tag{5.23}$$

2. Setting $v(z,\tau) = T(z,\tau) - U(z)$, using Eqn.5.14 and the boundary conditions, the following results,

$$\frac{\partial v(0,\tau)}{\partial z} = 0$$

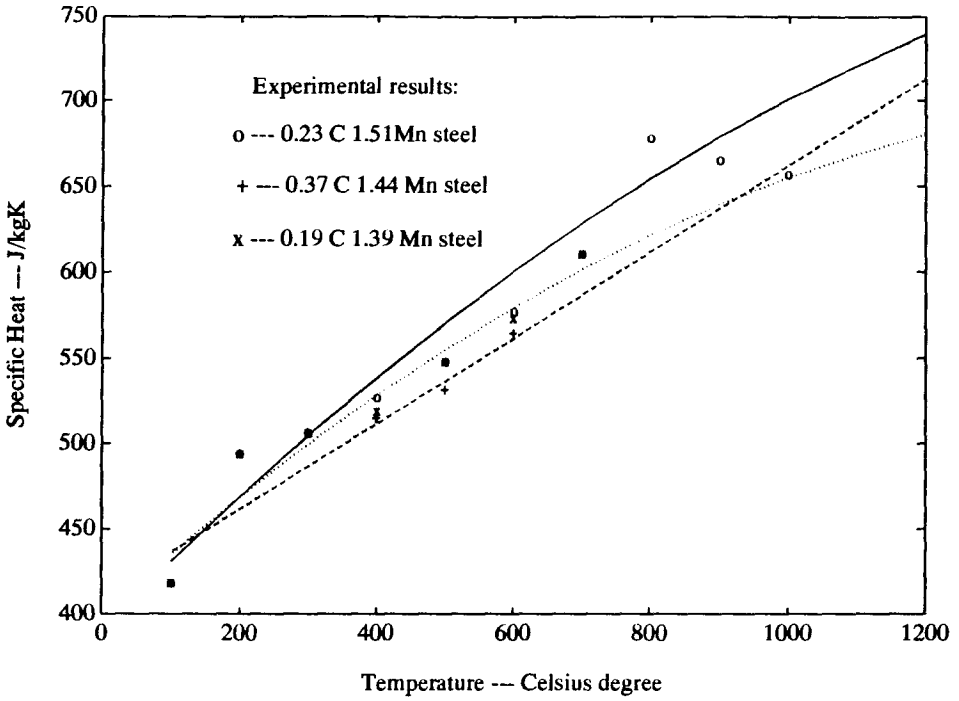

Figure 5.7: Specific heat as a function of temperature for C-Mn steels

$$\frac{\partial v(t,\tau)}{\partial z} + h_k v(t,\tau) = 0 \tag{5.24}$$
$$v(z,0) = T_0 - U(z)$$

where,

$$h_k = \frac{H(\tau)}{k_s} K = \frac{k_s}{\rho_w C_w} \tag{5.25}$$

3. Eqn.5.14 with homogeneous conditions of Eqn.5.24 has a solution as

$$v(z,\tau) = f(z) e^{-\lambda K \tau} \tag{5.26}$$

where,

$$K = \frac{k_s}{\rho_w C_w} \tag{5.27}$$

and λ is an eigenvalue and $f(z)$ is an eigenfunction of Sturn-Liouville problem:

$$\frac{\partial^2 f}{\partial z^2} + \lambda f = 0, \quad \text{with } \frac{\partial \mathrm{f}(0)}{\partial z} = 0 \tag{5.28}$$

The general solution to Eqn.5.29 is $f(z) = Asin(z\sqrt{\lambda}) + Bcos(z\sqrt{\lambda})$. Using the boundary condition, one may obtain $\sqrt{\lambda}sin(t\sqrt{\lambda}) = h_k cos(t\sqrt{\lambda})$, then we have

$$f(z) = Bcos(z\sqrt{\lambda}) \tag{5.29}$$

$$\sqrt{\lambda_n} = h_k cot(t\sqrt{\lambda_n}) \ \ (n = 1,\ 2,\ 3\ ...) \tag{5.30}$$

From Eqn.5.26, Eqn.5.29, Eqn.5.30,

$$v(z,\tau) = \sum_{n=1}^{\infty} B_n cos(z\sqrt{\lambda_n}) e^{-\lambda_n K\tau} \tag{5.31}$$

4. When $\tau = 0$, from Eqn.5.25,

$$T_0 - U(z) = \sum_{n=1}^{\infty} B_n cos(z\sqrt{\lambda_n}) \tag{5.32}$$

Using orthogonality,

$$\int_0^t [T_0 - U(z)] cos(z\sqrt{\lambda_n}) dz = B_n \int_0^t cos^2(z\sqrt{\lambda_n}) dz \tag{5.33}$$

B_n may be decided as,

$$B_n = \frac{2(T_0 - T_r) sin(t\sqrt{\lambda_n})}{t\sqrt{\lambda_n} + \frac{1}{2} sin(2t\sqrt{\lambda_n})} \tag{5.34}$$

So, finally the desired solution is

$$v(z,\tau) = \sum_{n=1}^{\infty} \frac{2(T_0 - T_r) sin(t\sqrt{\lambda_n})}{t\sqrt{\lambda_n} + \frac{1}{2} sin(2t\sqrt{\lambda_n})} cos(z\sqrt{\lambda_n}) e^{-\lambda_n K\tau} \tag{5.35}$$

5.4.6 Heat Transfer Coefficient at Workpiece-Roll Interface

Recent experiments[46] showed that the heat transfer coefficient at the workpiece-roll interface is a variable. In [46], when summarizing the experiments, it is stated that,

> The heat transfer coefficient is seen to vary from 17 to 57 kW/m^{2}K during the first 0.015 second in the roll gap and then to remain constant thereafter.

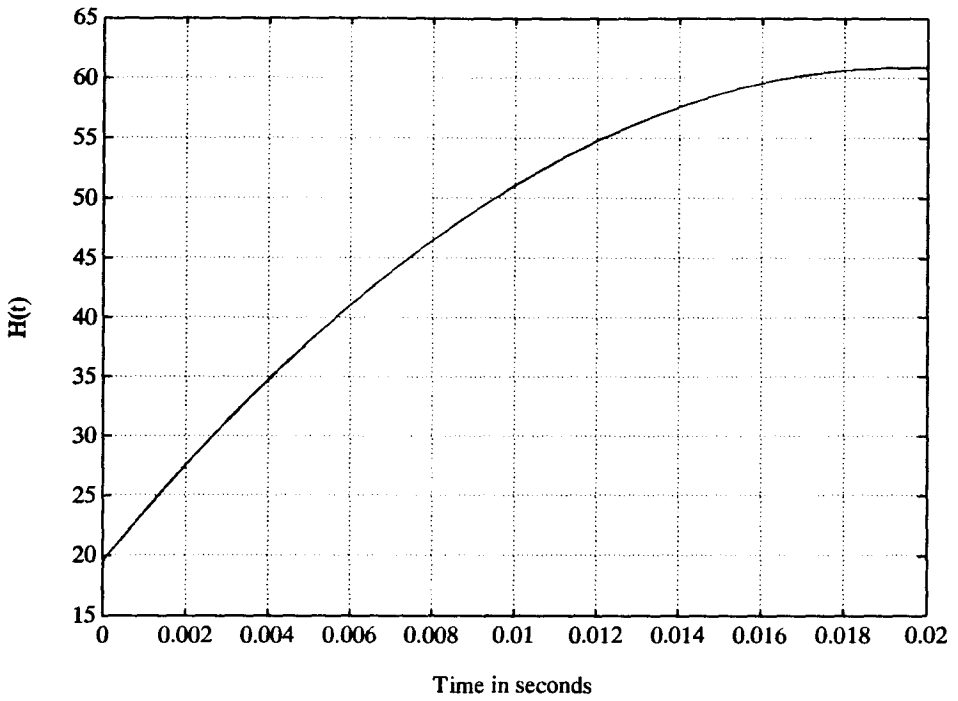

Figure 5.8: Example for heat transfer coefficient at workpiece-roll interface (lubricant: water)

> The progressive increase in the heat-transfer coefficient in the first 0.015 second is thought to be due to the decrease in contact resistance with the increase in specific rolling pressure, which reaches a maximum at the neutral point.

This may be the reason that the coefficient is expressed as a function of time in a more recent work[47] as the following,

$$H(\tau) = 19.561 + 42.47(10^2)\tau - 1.09(10^5)\tau^2 \qquad (\mathrm{kW/m^2K}) \qquad (5.36)$$

where τ is in seconds. Figure 5.8 shows the plot. It is clear that the transient period is very short. Therefore, in present study the coefficient may be taken as constant corresponding to the mean steady state value.

It should be noted that lubricants have significant effects on the magnitude of the coefficient. Using the results from compression tests in studying the contacts between high temperature (780 °C) specimens and low temperature specimens, Murata and his

Table 5.1: Heat-transfer coefficients at roll-gap interface for different lubricants

Lubrication condition	Heat-transfer coefficient, $kWm^{-2}K^{-1}$	
	No scale	Scale
No lubricant	29.1 - 34.9	7 - 10.6
Water	23.3 - 81.4	10.6
Hot-rolling oil	200 - 460	5.8
Hot-rolling oil+20% $CaCO_3$	69.8 - 175	12.8 - 23.3
Hot-rolling oil+40% $CaCO_3$	12.79 - 17.4	...
KPO_3	5.8	...

coworkers[49] calculated the heat transfer coefficients at the interface under different lubrication conditions, and suggested some useful values for hot rolling processes. The results are reproduced in Table 5.1.

Devadas et al[36] used 37 $kWm^{-2}K^{-1}$in their work. They stated that according to Stevens et al's estimation[50], the heat-transfer coefficient at the roll-gap interface is 37.6 $kWm^{-2}K^{-1}$during the first 30ms and 18 $kWm^{-2}K^{-1}$thereafter. They examined the coefficient in the range 30—50 $kWm^{-2}K^{-1}$, and concluded the following.

- A 25% variation in the coefficient causes a 2% change in surface temperature.
- 40% $CaCO_3$ in a hot-rolling oil reduces the coefficient to 13 $kWm^{-2}K^{-1}$from an average value of 50 $kWm^{-2}K^{-1}$for water lubrication. The difference of the surface temperature at the exit for the two cases is 175 °C.

These results should be taken into account in the VGR process design and the production. The present study uses water as coolant and an average value of 50 $kWm^{-2}K^{-1}$as the coefficient, so the roll surface temperature may be taken as around 100 °C.

5.4.7 Convection and Radiation

When the workpiece is moved out of furnace, temperature starts dropping because of convection and radiation. The method for estimating heat loss by convection and radiation used in this work is similar to that suggested in [44][45], which consists of two steps.

1. Establishing a model for one-dimensional flow

According to assumption 6 in Section 5.4.3, when taking its two pairs of the two parallel surfaces as infinitely large, an instantaneous heat balance of the bar in open air holds for each pair:

Rate of heat loss from surfaces = −rate of heat accumulating in the bar

Thus, we have the following equation,

$$2h_c A_s(T_s - T_a) + 2\epsilon B A_s(T_s^4 - T_a^4) = -\rho C_w V \frac{dT_s}{d\tau} \tag{5.37}$$

where T_a is the ambient temperature which, in comparison with the workpiece temperature, may be taken as zero. Assuming

$$S_b = \rho C_w \frac{V}{A_s} = \rho C_w L \tag{5.38}$$

where L will be substituted by either t or w. Eqn.5.37 becomes,

$$2(h_c T_s + \epsilon B T_s^4) = -S_b \frac{dT_s}{d\tau} \tag{5.39}$$

by rearranging,

$$-S_b^{-1} \int_{\tau_i}^{\tau_f} d\tau = \int_{T_i}^{T_f} \frac{dT_s}{2h_c T_s + \epsilon B T_s^4} \tag{5.40}$$

After integration and some tedious manipulation, the following results,

$$T_f = \left[\frac{\epsilon B}{h_c} \left\{ e^{2h_c S_b^{-1} \Delta\tau} \left(1 + \frac{h_c}{T_i^3 \epsilon B} \right) - 1 \right\} \right]^{-\frac{1}{3}} \tag{5.41}$$

where, $\Delta\tau$ is the time delay for temperature dropping to T_f; h_c is convection heat transfer coefficient and is chosen to use forced convective heat transfer correlations for flow over a plate.

Since the rolling velocity is not high and the cooling can be treated as laminar flow over isothermal plates, the average heat transfer coefficient is given by[48]:

$$h_c = 0.664 R_e^{0.5} P_r^{0.33} \frac{k_c}{L_c} \tag{5.42}$$

where R_e and P_r are the Reynolds and Prandtl numbers that are defined as usual; L_c is the characteristic length, determined as the length of the plate in contact with the air flow; k_c is the thermal conductivity of the air.

2. Establishing a model for two-dimensional flow

Using the idea introduced in [45], due to J. S. Langston, the following may be written,

$$\left(\frac{T_f}{T_i}\right)_{total} = \left(\frac{T_f}{T_i}\right)_{width} \left(\frac{T_f}{T_i}\right)_{thickness} \tag{5.43}$$

Substituting t_0 and w_0 or t_1 and w_1 into Eqn.5.38, respectively, corresponding values of S_b may be obtained. From values of S_b, one will be able to compute $(T_f)_{width}$ and $(T_f)_{thidkness}$ before the entry and after the exit. Thereafter, Eqn.5.43 may be solved under different conditions.

5.4.8 Mean Temperature of the Deforming Body in the Roll-Bite

With all the above relationships established, it is very convenient to compute the desired mean temperature for each pass.

Eqn.5.35 gives the temperature distribution along the z-direction at certain instant. By chosing a finite number of points equally spaced along z-axis, i.e., z_i, and time-axis — same as the x-axis —, i.e., τ_j, the mean temperature may be computed in the following

manner,

$$T_m = \frac{1}{n_i}\frac{1}{n_j}\sum_{j=1}^{n_j}\sum_{i=1}^{n_i} T(z_i, \tau_j) \tag{5.44}$$

which is similar to finite element analysis.

In this study, it is considered that accurate enough solution should be obtained by using $i = 10$ and $j = 20$.

5.5 Flow Stress Models

5.5.1 Model for Steels

The current analysis will consider low to medium operation speed with a strain rate range of 1-50s^{-1}, while the temperature may vary in the commercial hot rolling range, i.e., 800-1250 °C. The flow stress model used should apply to this conditions.

It can be easily found out in the literature that numerous researchers utilized the unified creep relationship that works well in hot rolling operations, which is the following,

$$\dot{\varepsilon} = A\,\sinh(\alpha\sigma)^{\mathrm{n}}\,\exp\left(-\frac{\mathrm{Q_a}}{\mathrm{R_g T}}\right) \tag{5.45}$$

or rearrange it,

$$Z = \dot{\varepsilon}\,\exp\left(\frac{Q_a}{R_g T}\right) = A\,\sinh(\alpha\sigma)^{\mathrm{n}} \tag{5.46}$$

where A, n and α are constants independent of temperature, Z is the well-known Zener-Holloman temperature compensated strain rate parameter.

A reasonable value of the activation energy, Q_a, for a wide range of C-Mn steels(0.05-0.68 C, 0.44-1.64 Mn), has been reported[52] to be approximately 312 kJ/mol, although it was observed that some variations did exist, such as 270 and 286 kJ/mol cited in [37]. Devadas[37] showed that both A and Q_a are variables of strain, though the variations are small.

Eqn.5.46 may be linearized as,

$$\frac{Q_a}{R_g T} + \ln\dot{\varepsilon} = \ln A + n\ln[\sinh(\alpha\sigma)] \tag{5.47}$$

The empirical constants may be determined by holding either the strain rate or the temperature as a constant and using the experimental data(further explanation on the procedures to determine the constants is given in Section 6.1.1). For C-Mn steels, the data published in [53] are used in present study.

In order to incorporate the data in the computer algorithm, a fairly large amount of data is read from [53], and then fitted by least square approximation into some 80 different polynomials, each of which is within 5th to 7th order and is in a matrix form. Figures B.1—B.4 in Appendix B show the fitting results. Such a wide range of data is needed to suit the variation in the C and Mn composition, and the variation of the temperature, strain and strain rates. Such a data-base is also convenient for interpolation or extrapolation in determining Eqn.5.45.

5.5.2 Using Lead as a Modelling Material

It is undisputed that an accurate flow stress model is absolutely necessary for a desirable solution to the hot rolling problem. Unfortunately however, since it is generally not feasible to obtain such information from production mill trials, a complete set of data on the deformations of various metals under the processing conditions does not exist. "It was observed that lead strain hardens in a similar manner to steel at elevated temperatures, and that the static softening behavior can be modelled using equations similar to these for C-Mn and stainless steels."[54], Hence the laboratory techniques of simulation and modelling have been developed by using commercially pure lead [54][55].

It should be noted here that lead can be only used to simulate the dimensional changes during hot rolling, but not the temperature effects on the rolling loads. However, using

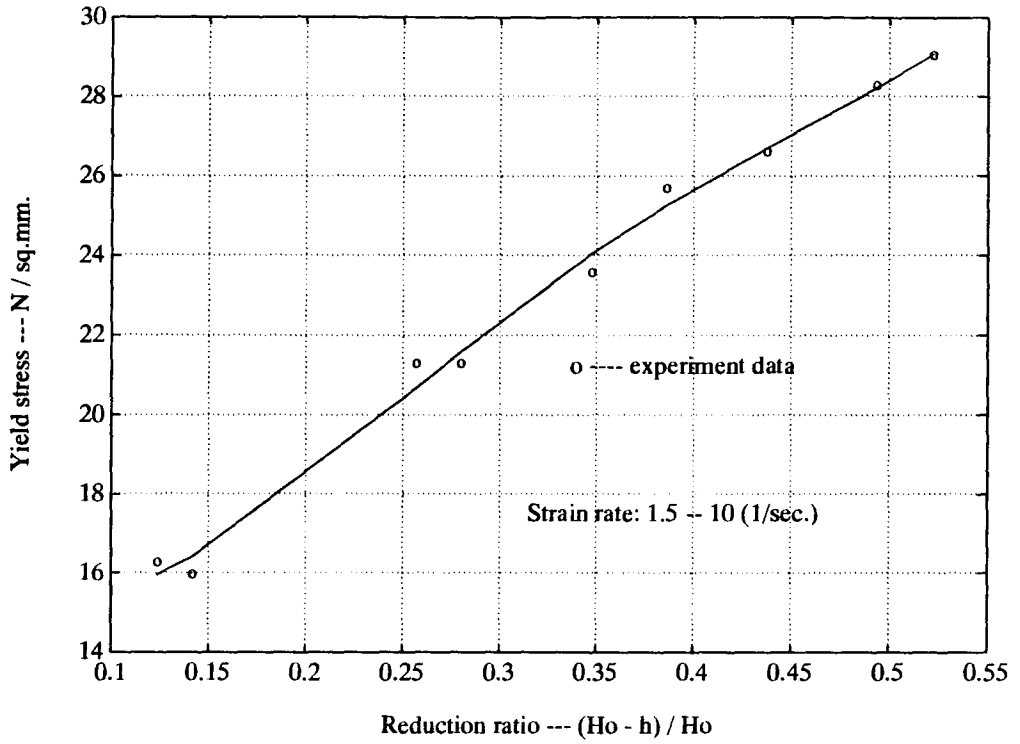

Figure 5.9: Flow stress model: the correlation between yield-stress and reduction ratio of pure lead. Data source: [56]

lead as a modelling material may be a good approach to reduce the experimental errors to minimum caused by the thermal effects and the difficulties in handling when operating at high temperature.

The data used in [55] came from [56], which was the only source that can be found at this time providing a wide range of compression testing data. By using least square data fitting technique, the following stress model is obtained,

$$\sigma = 742.5r^4 - 1028.9r^3 + 485.2r^2 - 55.8r + 17.2 \tag{5.48}$$

and figure 5.9 shows the fitting results.

In Eqn.5.48, instead of using strain as variable, the reduction ratio, r, is used, which was the testing results before conversion.

Chapter 6

MODEL VERIFICATION

In the above chapters, a complete model for implementing the VGR process has been fully described, which consists of the deformation model, the flow stress model and the temperature model. It is important that these models be verified in experiments before the machine design process may be carried out. Due to the lacking of the experimental equipments, a complete set of testing data, regarding a certain workpiece composition, temperature changes, strain-stress correlations, roll force and torque, etc., is not available. Nevertheless, the model may be verified separately, by using some appropriate data reported in the literatures.

6.1 Flow Stress Model Verification

6.1.1 Empirical Constants in Flow Stress Model

The linearized flow stress model, Eqn.5.47, is used to determine the empirical constants, A, n and α. Due to the availability of experimental data, C-Mn steel is used for a sample calculation. A value of 312 kJ/mol for the activation energy, Q_a, is chosen, as is explained in Section 5.5.1.

By holding T as a constant, n and A may be determined graphically by the relationship between $\ln(\sinh(\alpha\sigma))$ and $\ln \dot{\varepsilon}$. The results are shown in figure 6.1. Or similarly, by holding $\dot{\varepsilon}$ as a constant, figure 6.2, n and A may be determined by the relationship between $\ln(\sinh(\alpha\sigma))$ and $1/T$. It is observed, after many testing runs in the simula-

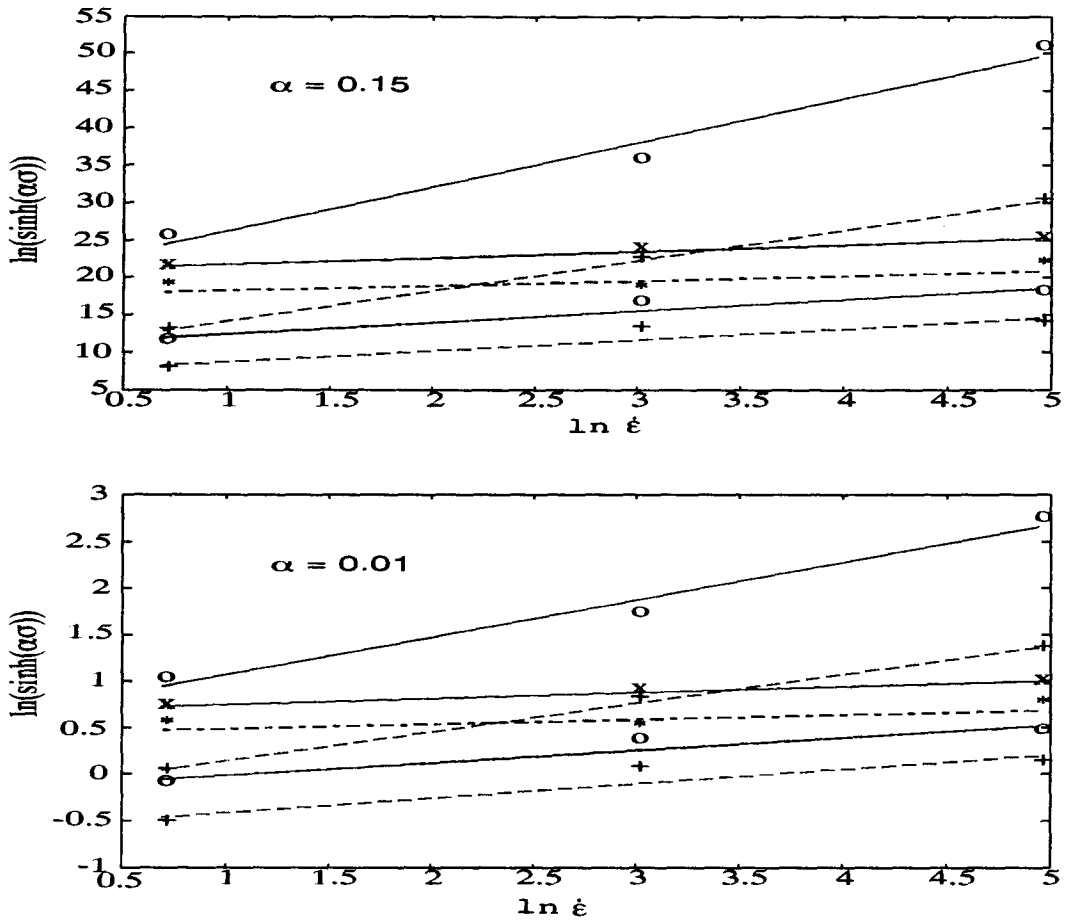

Figure 6.1: Relationship between $\ln(\sinh(\alpha\sigma))$ and $\ln \dot{\varepsilon}$ for a C-Mn steel (0.03 C 0.62 Mn) at a strain of 0.35. Experimental data: o — ($\dot{\varepsilon} = 2s^{-1}$), * — ($\dot{\varepsilon} = 20s^{-1}$) and + — ($\dot{\varepsilon} = 140s^{-1}$). Data source: [53].

tion with different values of α, that the magnitude of α has no effect on the final stress calculation. In other words, the value for α may be arbitrarily chosen.

Note that, since the experimental data shows significant irregularity in the flow stress of this type of steel, the slopes in different regions of the relationship, $\ln(\sinh(\alpha\sigma))$ — $\ln \dot{\varepsilon}$ or $\ln(\sinh(\alpha\sigma))$ — $1/T$, are not the same. So n and A are no longer constants. This results in a complication in the modelling.

It is also confirmed that, when holding α as a constant, both n and A are non-linear

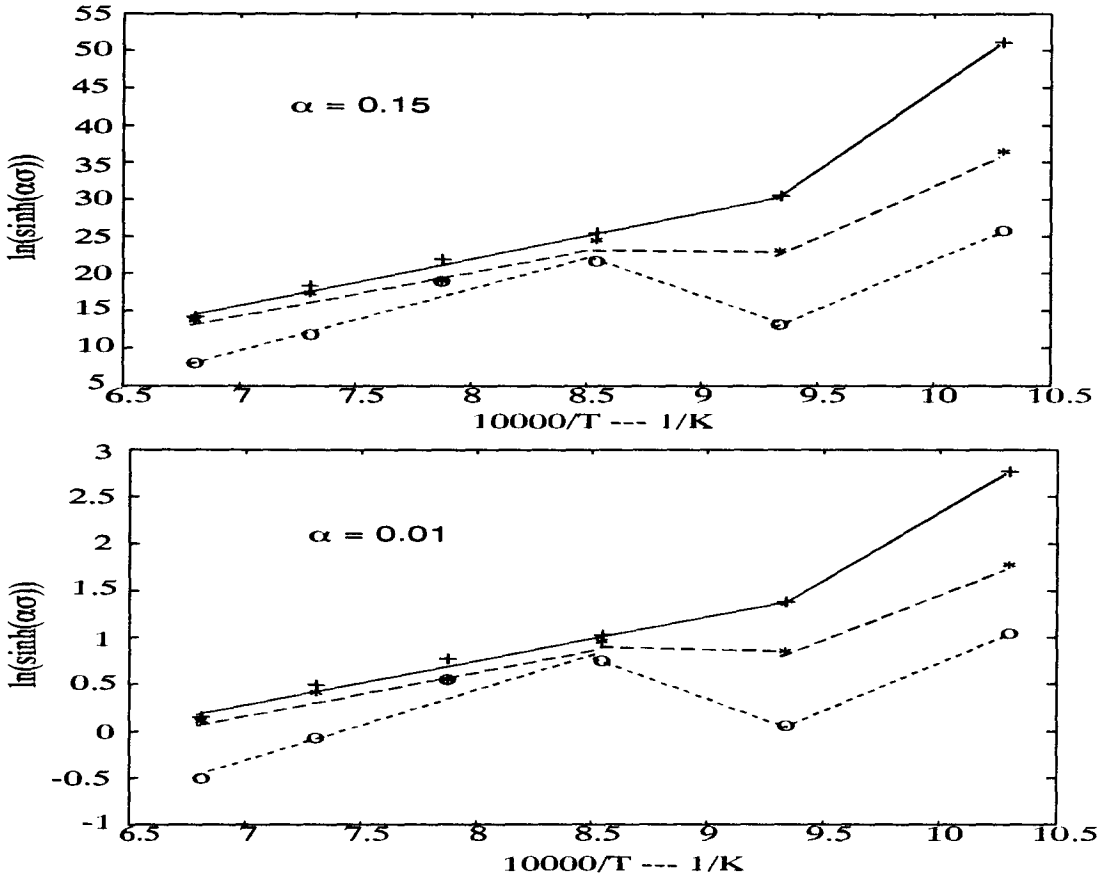

Figure 6.2: Relationship between $\ln(\sinh(\alpha\sigma))$ and $1/T$ for a C-Mn steel (0.03 C 0.62 Mn) at a strain of 0.35. Experimental data: o — ($\dot{\varepsilon} = 2s^{-1}$), * — ($\dot{\varepsilon} = 20s^{-1}$) and + — ($\dot{\varepsilon} = 140s^{-1}$). Data source: [53].

functions of strain and temperature, which can not be written in a simple analytical expression. In order to calculate the instantaneous values of n and A, the two non-linear functions were established by a computer program based on a simple surface fitting algorithm[59]. A brief description of the algorithm follows.

1. Assuming the surface is a two dimensional polynomial,

$$\begin{aligned} [n \quad \ln A] &= f(\varepsilon, T) \qquad (6.1) \\ &= a_0 + a_1\varepsilon + a_2 T + a_3\varepsilon^2 + a_4\varepsilon T + a_5 T^2 + \end{aligned}$$

$$a_6\varepsilon^2 T + a_7\varepsilon^3 + a_8\varepsilon^3 T^2 + ... \tag{6.2}$$

where a_i $(i = 0,1,2, ...)$ are constants to be determined, and by holding temperature as a constant, an one dimensional polynomial may be obtained,

$$[n \quad \ln A] = b_0 + b_1\varepsilon + b_2\varepsilon^2 + b_3\varepsilon^3 + ... \tag{6.3}$$

where b_i $(i = 0,1,2, ...)$ are constants to be determined.

2. Use Eqn.6.3 to generate enough points at certain strains, including the desired strains points.

3. Repeat the first two steps at different typical temperatures.

4. By holding strain at the desired value to interpolate n and $\ln A$ along temperature direction, n and $\ln A$ as functions of temperature at the desired strain is then established.

6.1.2 Determination of Flow Stress at any Desired Conditions

With the establishment of functions for n and A, Eqn.5.46 may be rearranged as the following,

$$\sigma = \frac{1}{\alpha}\sinh^{-1}\left[\frac{\dot{\varepsilon}\exp\left(Q_a R_g^{-1}T^{-1}\right)}{A}\right]^{\frac{1}{n}} \tag{6.4}$$

Now, by using Eqn.6.1 to calculate the values of n and A at the required strain and temperature, the parameters in Eqn.6.4 may all be determined. So σ may be determined for that point, $(\varepsilon, \dot{\varepsilon}, T)$. Note that a value for α has to be chosen when determining Eqn.6.1.

Figure 6.3 shows a comparison between the model prediction and experimental data for a certain steel. For the working range of the VGR process, i.e., a strain rate

range of 1—50s^{-1}, a temperature range of 800—1250 °Cand a strain range of 0.051—0.693(reduction ratio 8% - 50%), the errors in the model prediction are within 5%. It is noticed that at 700 °C, the errors are larger. This may be a confirmation to a remark by Hosford and Caddell[60]: such correlations as Eqn.5.46 "may break down if applied over too large a range of temperatures, strains, or strain rates".

6.2 Temperature Model Verification

6.2.1 Verification Using Data from Conventional Rolling

The testing data in [37] for workpiece surface temperature and the same set of data of the rolling conditions have been used in order to solve for the temperature model, Eqn.5.22, 5.41 and 5.43. It is found out that the converging speed of Eqn.5.35 is largely dependent upon the size of time steps and the magnitude of the rolling speed. The smaller the size of the time step and the faster the rolls rotate, the slower Eqn.5.35 converges, and vice versa. The calculation of the first node converges very slowly. As the calculation moves on to the second and the rest nodes, the equation converges faster and faster.

Figure 6.4 shows the simulation results. For the grid shown and for a converging accuracy of 0.1 °C, the number of terms taken in calculating Eqn.5.35 for the first node is 97, and for the last node is 9. This results in a relatively long time in computation.

The mesh plot shows the roll chilling effects clearly. The temperature gradients only exist in the 4-5 layers to the surface. Such a shallow gradient is due to the high rolling speed(note that only about 33 milliseconds of in-bite time).

In the surface temperature prediction, large errors, compared to the experimental data, exist in the first few nodes, which most likely are caused by taking a contact of 50($kWm^{-2}K^{-1}$) for the heat transfer coefficient at the interface between the workpiece and rolls, $H(\tau)$. As is indicated in figure 5.8, $H(\tau)$ is very small at the beginning, which

would result in a very small temperature gradient at the first few nodes, as confirmed by the experimental data. For the rest of the nodes, good agreement is obtained.

It should be indicated that such a fine grid as was used in simulation is not necessary for real applications. Besides, for the VGR process, the rolling speed will be much slower. These would contribute to a significant reduction in computing time.

6.2.2 Simulation of First Pass in VGR Process

In order to further verify the capability of the model, simulations for the mean temperature distribution along a whole workpiece during and after the first pass of the VGR process have been carried out.

The simulation follows the sequence in a real production. That is, first, allowing 5 seconds for transferring the workpiece from furnace(1200 °C) to the mill, the actual entrance temperature may be calculated by the radiation and convection model. Then rolling starts and the temperature at each node in the roll-bite is calculated by the conduction model, while continuing the estimation of temperature drop in the workpiece outside the entrance.

At the exit, the mean temperature is estimated by averaging the temperature at the nodes in vertical direction. And then, right out of the exit, starts the radiation and convection calculation again to count in the temperature drop. Finally, allows 5 seconds handling time for the workpiece to be transferred to the entrance for second pass.

Figures 6.5 and 6.6 are the results from three different runs, showing the effects of varying rolling conditions on a same workpiece. The same heat transfer coefficient(50 $kWm^{-2}K^{-1}$) at the interface between workpiece and rolls used in the last Section was chosen. Some enlightening observations for this particular workpiece and working temperature range may be summarized in the following.

1. The rate of temperature drop due to radiation and convection is about 2 - 3 °C/sec.

2. The mean temperature drop is mainly due to conduction in the roll-bite. This again confirms that the roll chilling effects is dominant. The higher reduction ratio, the larger the amount of mean temperature drops. Since higher reduction ratio implies longer time contacting to the rolls.

3. Increasing the rolling speed reduces the contacting time between the workpiece and the rolls, which results in smaller amount of temperature drop.

4. There are two different ways of increasing the rolling speed. One is to increase roll diameter(case B in figure 6.5). The other is to increase roll velocity(case C in figure 6.5). It is clear from figure 6.5 that the second method(case C) is preferred, because in that way the contact length l is not increased.

5. Figure 6.6 shows the mean temperature in the roll-bite along the whole pass. Again, it shows that case C(the top curve) is preferred, as smaller changes in mean temperature is resulted, which, in turn, would result in smaller variations in flow stress. The calculations were performed by Eqn.5.22 and 5.44.

The above observations are important and may serve as guidelines in the VGR process implementation.

6.3 Deformation Model Verification

6.3.1 The Side Spread Estimation

In Chapter 4, a deformation model based on upper bound theorem has been worked out. As has been explained in Section 5.2, when looking merely at the deformation, the material may be assumed rigid perfectly-plastic. This means that the flow stress becomes

a proportional constant and has no influence on the amount of side spread. Figure 6.7 shows the results from the simulation run and a comparison is made with the data from [55]. The agreement is excellent.

6.3.2 Torque Estimation

The total net power consumption is given by the minima of Eq.4.3, and torque may be calculated from the following equation,

$$M = \frac{R}{V_R} J^*_{min} \tag{6.5}$$

Figure 6.8 gives the results from the simulation run and a comparison is made with the data from [57]. The agreement is very good, as is expected that the results from Eq.4.3 should be the *upper bound.*

6.3.3 Roll Separating Force Estimation

Traditionally, the upper-bound approach can not be directly used in determining the rolling force. The reasons are apparent — the frictional force at the interfaces changes direction due to the changes in relative speeds between the rolls and the workpiece, and there is very little knowledge on this particular subject available.

It is unfortunate that, one may find out in the literature, many researchers had to use the slab method to calculate the roll force, when everything else had been worked out by the upper bound approach. Since slab method can only be used under plain strain condition, some researchers, such as [20][6], after devoted painstaking efforts in three dimensional solution through upper bound approach, chose to further simplify the problem into a two dimensional one so the slab method can be used for the solution to the roll force. This resulted in inconsistency in the theoretical analysis and may be considered a shortcoming of the UBA approach.

In order to overcome such a difficult situation, a concept called equivalent coefficient of friction(μ_{eq}), similar to the one proposed by D. Y. Yang and J. S. Ryoo[58] when ring rolling process was investigated, will be adopted.

This coefficient is defined as the ratio of the frictional force(F_T), which is the difference between the foreward friction and the backward friction, to the overall radial force(F_R) upon the rolls, figure 6.9. That is,

$$\mu_{eq} = \frac{F_T}{F_R} \tag{6.6}$$

where F_T is also the tangential force on the rolls. Accordingly,

$$F_T = \frac{M}{2R} \tag{6.7}$$

Therefore, if μ_{eq} were determined by experiments, the roll separating force may be determined by using Eqn.6.5, 6.6 and 6.7 as,

$$F = \sqrt{F_T^2 + F_R^2} \tag{6.8}$$

Since the actual friction is affected by various factors, such as surface conditions, roll size, temperature, workpiece dimension, etc., it is virtualy impossible to obtain the exact distribution of friction. By considering the overall friction effect on the roll force and torque, the extremely complicated situation is simplified. The value of μ_{eq} may be determined from a set of measurements for the roll force and torque, as suggested in [58].

Note that geometrically(figure 6.9)

$$\mu_{eq} = \tan\theta = \frac{x_d}{\sqrt{R^2 - x_d^2}} \tag{6.9}$$

then, there must be $0 < x_d < l$. As the normal pressure is not uniformly distributed along the contact length(l), the value of x_d has to be determined experimentally. This may suggest another approach in computation.

In the present study, the experimental results for roll force and torque reported in [57] are used as a demonstration, and the values of μ_{eq} are computed for the same set of data as was used in computing the torque(Section 6.3.2). Figure 6.10 shows the simulation output. For the same reason as described in Section 5.5.2, lead was chosen as the experimental material, and the flow stress model, Eqn.5.48, is used. For reduction ratios ranging from 8% — 50%, the best results are obtained when the values of μ_{eq} were chosen as a variable within 0.108 — 0.135, which gives the values of the ratio, x_d/l, within 0.8506 — 0.4285.

6.4 Concluding Remarks

6.4.1 Summary and Conclusions

A complete mathematical model for implementing the VGR process under hot working conditions has been established through a fundamental analysis. The model takes into account the three major aspects of the process that the machine designers and the production engineers have to deal with.

1. The deformation model is capable of producing the upper bounds of the rolling loads, namely, the roll separating force and the torque, that will be needed in machine design task. Using the model, the instantaneous rolling loads, which are important information for the roll-gap control, can also be obtained with the help of accurate flow stress data.

   The force calculation is based on a new concept called the equivalent coefficient of friction, μ_{eq}. The adoption of this concept leads to two significant advantages. Firstly, the tests for the actual friction coefficient at the interface between the rolls and the workpiece, as in the traditional rolling process, may be avoided. It is known

that there is no reliable method for such testing. Besides, the available methods usually involve many facilities that are costly, time consuming and inconvenient in practice. The test(See Section 6.3.3) to the μ_{eq}, however, will be very simple and reliable.

Secondly, this concept leads to a theoretical consistency in the application of the upper bound approach. Further simplifications are no longer needed, as were done by some researchers(See Section 6.3.3).

Another new feature related to the deformation model is that a simpler velocity field solution has been proposed. This largely reduced the work in derivation and computation. By such a velocity field, the side spread predictions were shown to be successful.

2. A temperature model has been formulated based on one-dimensional flow assumptions in the roll-bite and two-dimensional flow outside the roll-bite. The model is capable of predicting the through-thickness temperature distribution in the roll-bite, estimating the mean temperature of the deforming body that is one of the important inputs to the flow stress model, and roughly calculating the the mean temperature distribution along the workpiece.

   Based on the mean temperature of the workpiece, roll pass scheduling may be performed, along with the side spread estimation. Some preliminary estimation of the final properties of the rolled products may also be possible.

3. The modelling of flow stress for steels is very involved. An accurate flow stress model, which is of great importance in implementing the VGR process, has been chosen. It has been shown that the unified creep relationship, Eqn.5.45, works very well, as is widely reported in the literature.

It is observed that, for the certain type of C-Mn steel used in this work, the parameters, n and A are non-linear functions of strain and temperature. Such functions may be determined by numerical methods.

Also, the value of 312 kJ/mol for the activation energy, Q_a, has been selected, as was reported in the literature. It worked well in this study.

6.4.2 Suggestions for Further Work

1. Further study of the equivalent coefficient of friction by experiments is needed. Without experiments, it is difficult to decided the actual range of this variable.

2. A temperature model for the rolls is needed in order to estimate accurately the temperature changes of the rolls. Although many reasons that in this study the temperature of rolls was assumed as a constant is given in Section 5.4.1, attempts can still be made.

3. The final microstructure of the rolled products will be another issue in the VGR process planning. A mathematical submodel of this purpose may be incorporated in the present model.

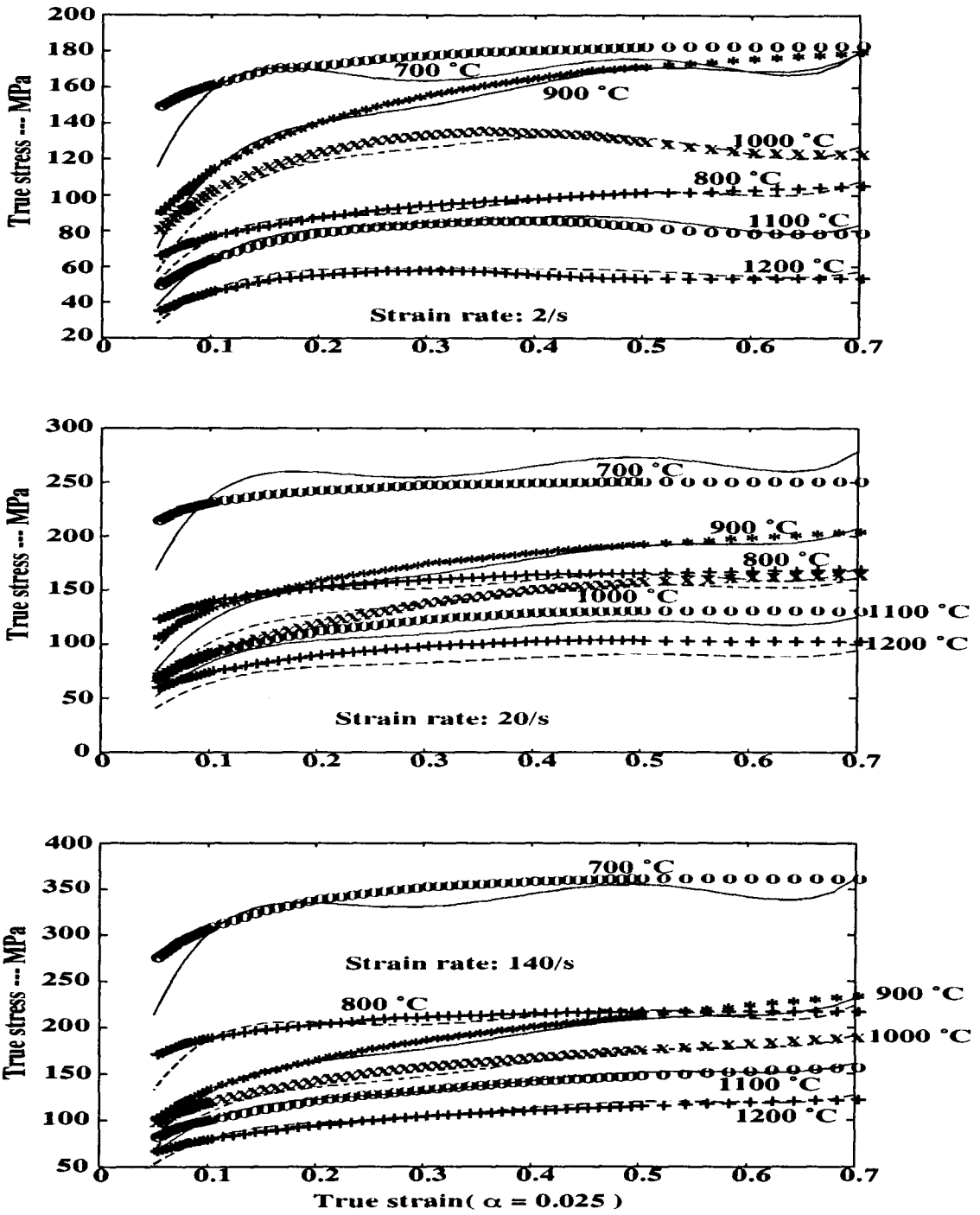

Figure 6.3: Flow stress model verification: C-Mn steel (0.03 C 0.62 Mn). Data source: [53]. +, *, x — experimental data. Solid or dotted lines — model predictions.

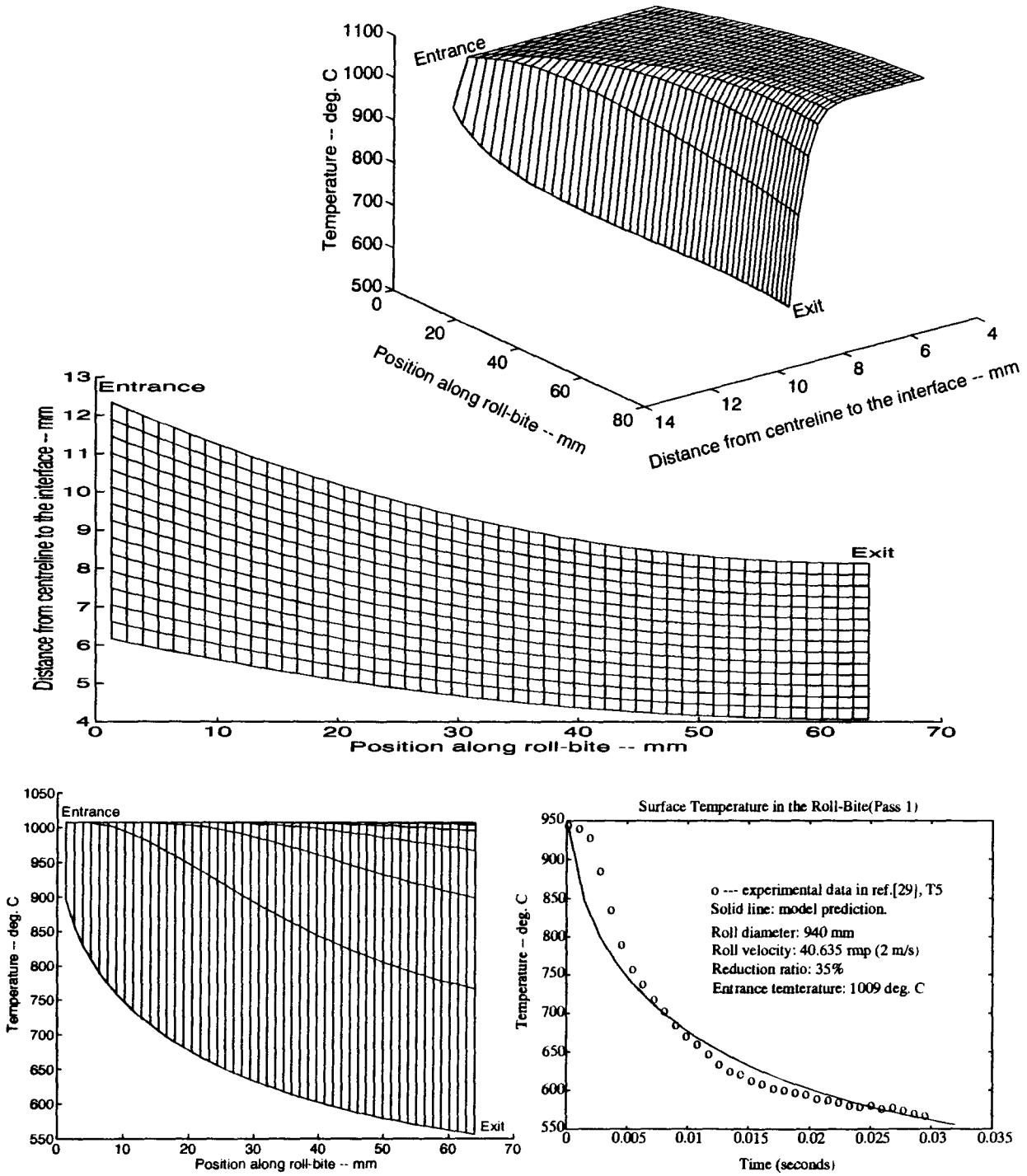

Figure 6.4: Temperature distribution in roll-bite. Data source:[37]. Top: 3D-mesh plot. Middle: grid used. Lower left: front view of the 3D-mesh. Lower right: surface temperature comparison. Reduction ratio: 35%. Entry temperature: 1012 °C.

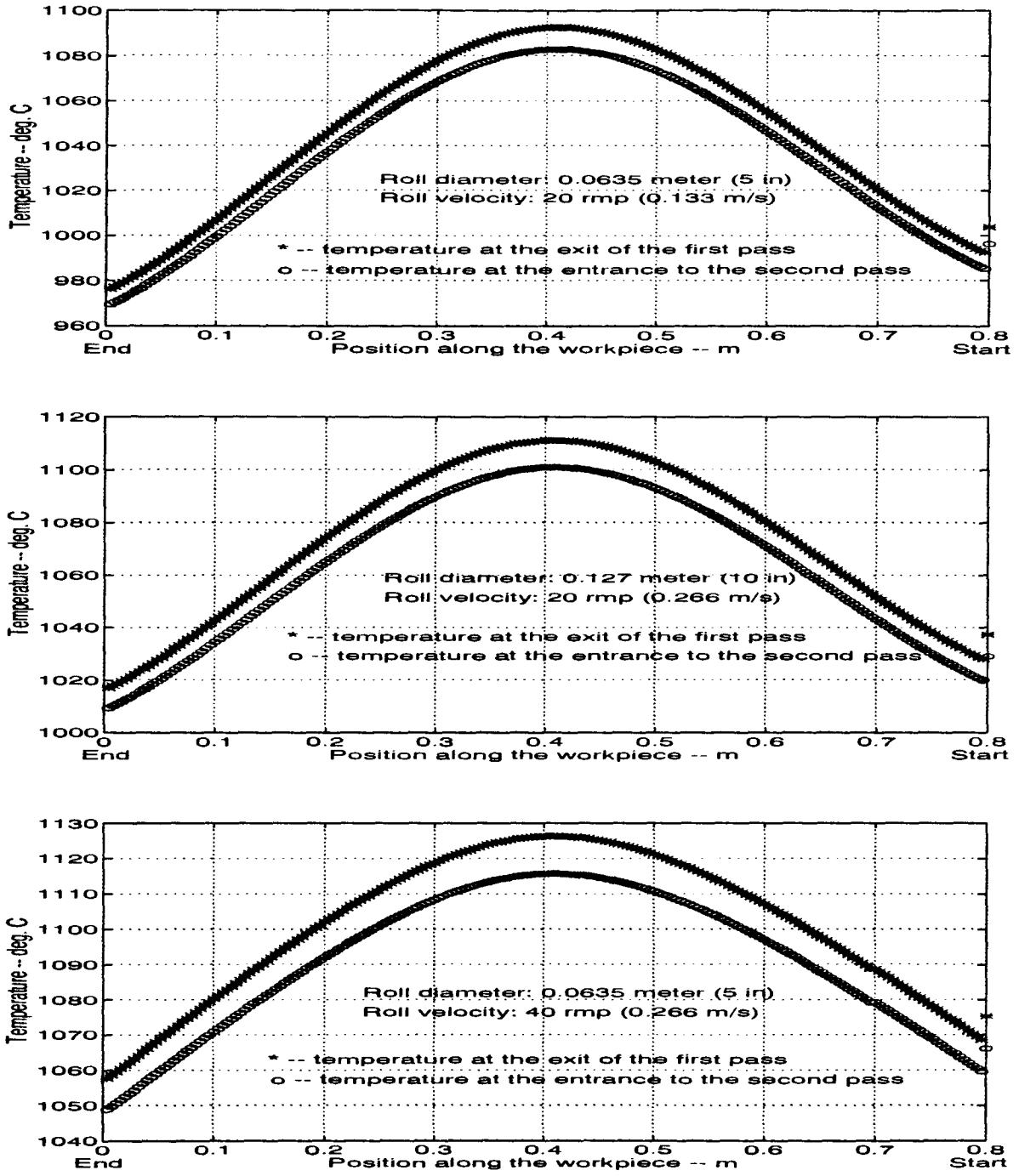

Figure 6.5: Sample calculation: mean temperature distribution of the workpiece for three different rolling conditions. Workpiece dimension(before rolling): 21.6 × 21.6 × 800mm. Reduction ratio: 8% — 50.8%. Furnace temperature: 1200 °C. Top(case A), time for pass1: 6.015 sec. Middle(case B), time for pass1: 3.008 sec. Bottom(case C), time for pass1: 3.008 sec.

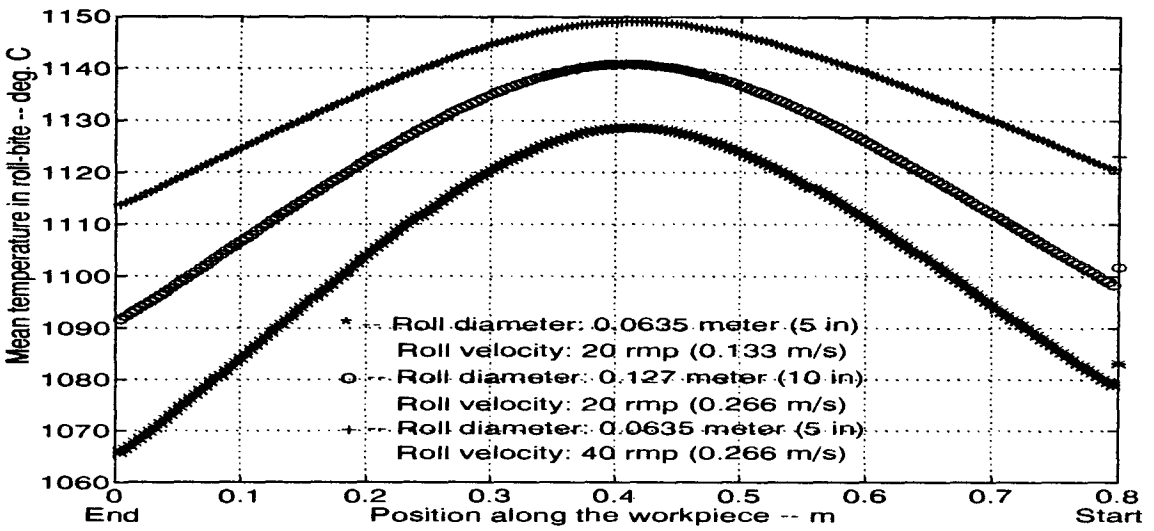

Figure 6.6: Sample calculation: effects of changes in geometry and roll velocity on mean temperature of the deforming body in the roll-bite during the first pass. Furnace temperature: 1200 °C. Workpiece dimension(before rolling): 21.6 × 21.6 × 800mm. Reduction ratio: 8% — 50.8%.

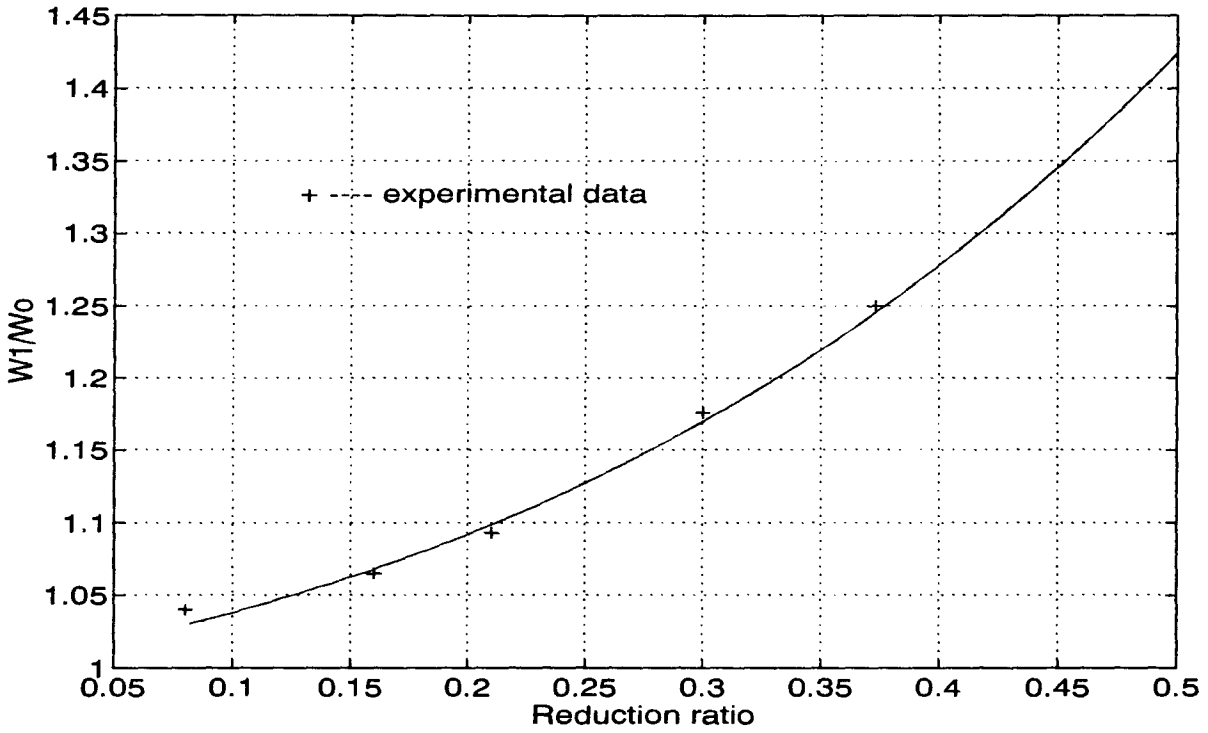

Figure 6.7: Spread prediction — comparison between simulation results and experiments[55]. Roll diameter: 101.6 mm(4 in). Specimen dimension: 9.525 × 9.525 mm(0.375 × 0.375 in).

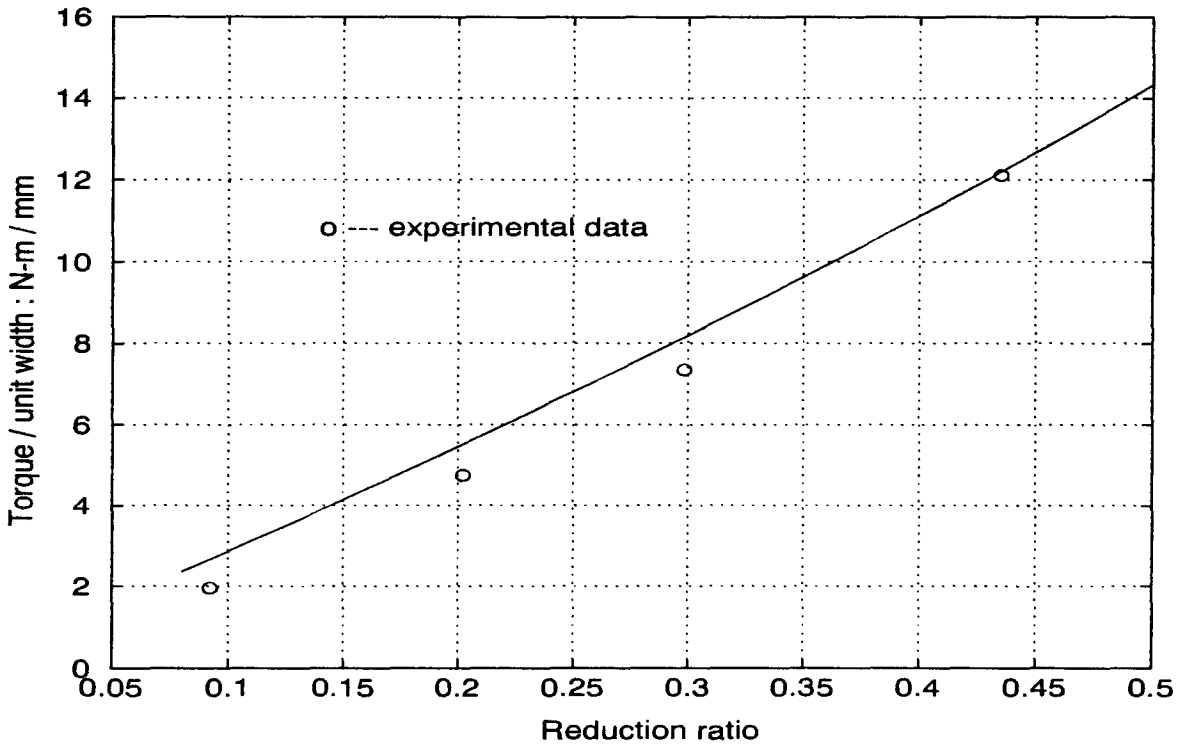

Figure 6.8: Torque prediction: comparison between simulation results and experiments[57]. Roll diameter: 127 mm(5 in). Specimen dimension: 12.7×19.05 mm(0.5×0.75 in).

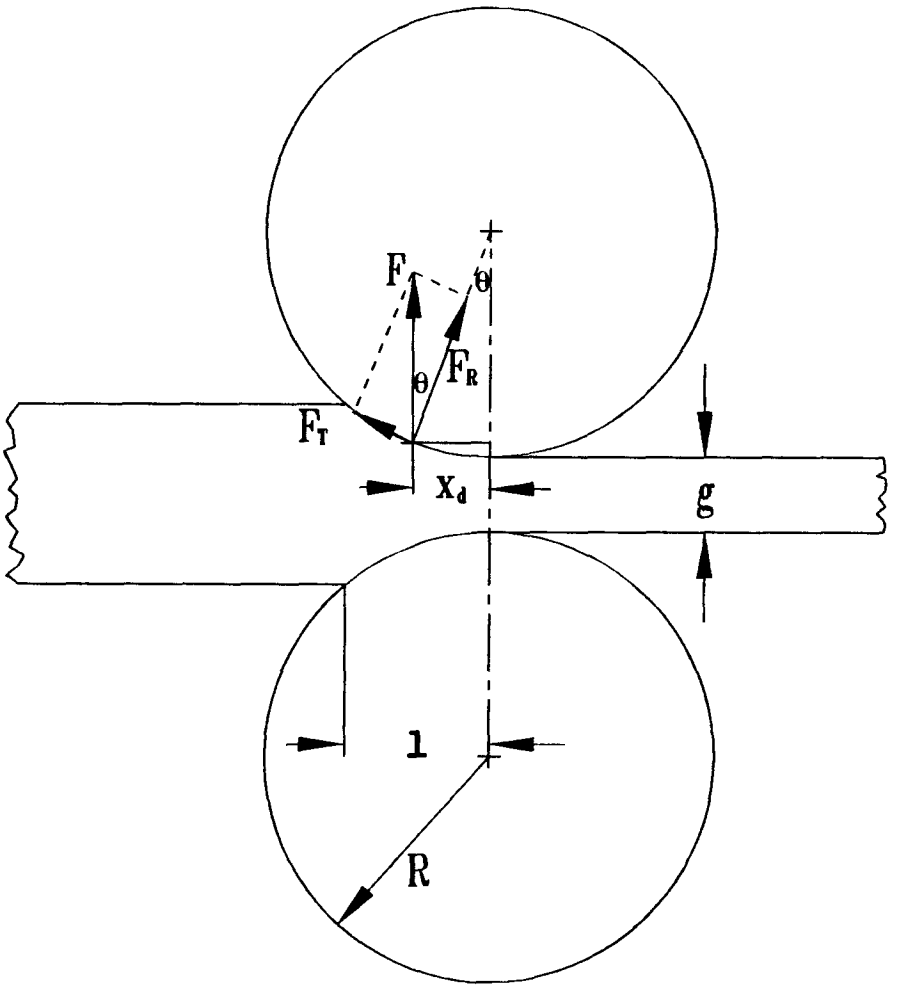

Figure 6.9: Schematic illustration of the roll force vectors layout in flat rolling process

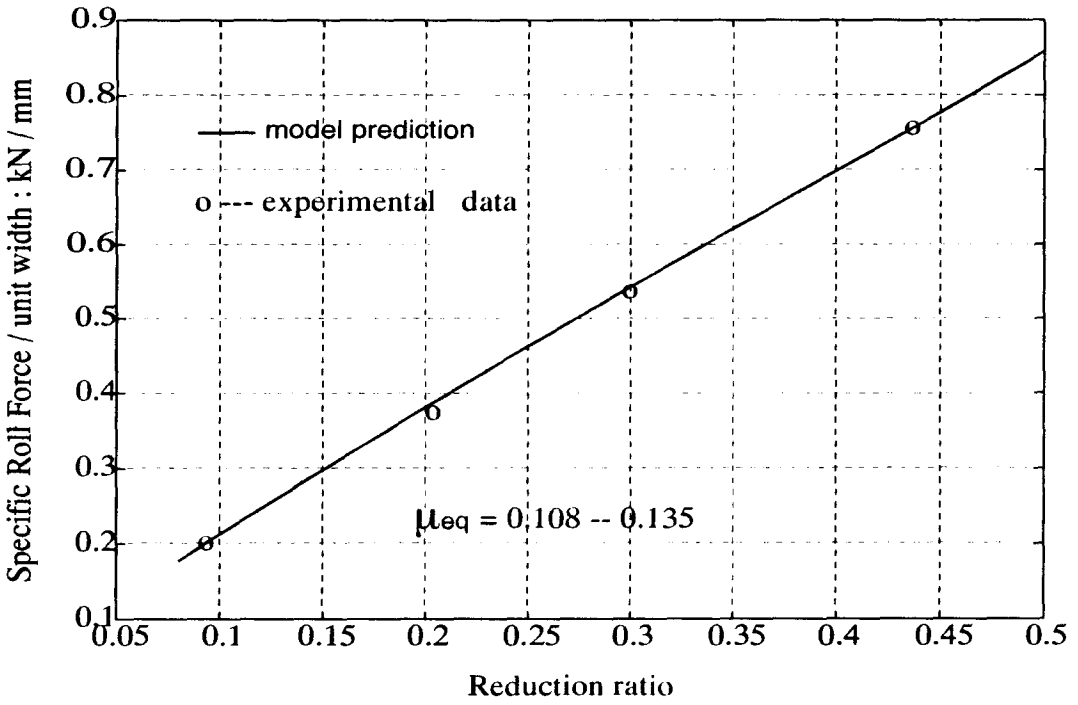

Figure 6.10: Roll force prediction: comparison between simulation results and experiments[57]. Roll diameter: 127 mm(5 in). Specimen dimension: 12.7×19.05 mm(0.5×0.75 in).

Bibliography

[1] Roberts, W. L., *Cold Rolling Of Steel*, Marcel Dekker, INC.1978.

[2] Theocaris, P.S., "A Study of the Contact Zone and Friction Coefficient in Hot-Rolling", *Metal Forming and Impact Mechanics*, Pergamon Press, Ed. by S.R. Reid, 1985

[3] Hill, R., "A General Method of Analysis for Metalworking Processes", *Mech. Phys. Solids*, Vol. 11, 1963, pp. 305.

[4] Lahoti, G. D., Kobayashi, S., "On Hill's General Method of Analysis of Metalworking Processes", *International Journal of Mechanical Sciences*, Vol. 16, 1974, pp. 521-540.

[5] Oh, S. I., Kobayashi, S., "An Approximate Method For A Three-Dimensional Analysis of Rolling", *International Journal of Mechanical Sciences*, Vol. 17, 1975, pp.293-305.

[6] Kennedy, K. F., "A Method for Metal Deformation and Stress Analysis in Rolling", *Doctoral Dissertation*, The Ohio State University, 1986.

[7] *Design And Application Of Leaf Springs — SAE J788a Handbook Supplement*, 1978.

[8] Sepehri, N., "Computer-Aided Rolling of Parts With Variable Rectangular Cross-Section", *MASc. Thesis*, The University of British Columbia, 1986.

[9] Sassani, F., Sepehri, N., "Prediction of Spread in Hot Flat Rolling under Variable Geometry Conditions", *J. Materials Shaping Texhnology*, Vol. 5, No. 2, pp.117-123, 1987.

[10] Sassani, F., Sepehri, N., "Computer-Aided Process Planning for Rolling of Parts Having Smoothly Varying Rectangular Cross-Section", *Int. J. Mach. Tools Manufact.*, Vol. 29, No. 2, pp.257-266, 1989.

[11] Sparling, L. G. M., "Formula for Spread in Hot Flat Rolling", *Proc. Inst. Mech. Engrs.*, Vol. 175. pp. 604-640, 1961.

[12] El-Kalay, A. K. E. A., Sparling, L. G. M., "Factors Affection Friction and their Effects upon Load, Torque, and Spread in Hot Flat Rolling", *J. Iron Steel Inst.*, Feb. 1968, No. 206, pp. 1110-1117.

[13] Chitkara, N. R. and Johnson, W., "Some Experimental Results Concerning Spread in the Rolling of Lead", *Journal of Basic Engineering*, Vol. 88, pp. 489-499, 1966.

[14] Takahashi, J., Sato, T., Sakai,Y., and Ayada, M., "Production of Taper Leaf Spring By S.P.M.",UDC 621.771.07, 1980.

[15] Hawkyard, J. B., Johnson,W., Kirkland, J., Appleton, E., 1973 "Analyses for roll force and toque in ring-rolling, with some supporting experiments", *Int. J. Mech. Sci.* **15**, pp.873-893.

[16] Kobayashi, S., Oh, S., Altan, T., *Metal Forming and the Finite-Element Method*, Oxford University Press, 1989.

[17] Hill, R., *The Mathematical Theory of Plasticity*, Clarendon Press, Oxford, 1950.

[18] Li, G.-J., Kobayashi, S., "Spread Analysis in Rolling by the Rigid-Plastic Finite Element Method", *Numerical Methods in Industrial Forming Processes*, p.777, Pineridge Press, Swansea UK, 1982.

[19] Grober, H., "Finite Element Simulatoin of Hot Flat Rolling of Steel", *NUMIFORM 86 — Numerical Methods in Industrial Forming Processes*, ed. by Mattiasson, K., *et al*, p.225, 1986.

[20] Lahoti, G.D., Akgerman, N., Altan, T., "Computer-aided analysis and design of the shape rolling process for producing turbine engine air-foils", Final report, 1978 December, *Contract Nas 3-20380.*

[21] Sevenler, S., Raghupathi, P. S., Altan, T., "Spread and bulge in Bar and Rod Rolling Using Flat Rolls", *Iron and Steel Engineer*, March 1986, pp. 57-62.

[22] Yih, C. S., "Stream Functions in Three-Dimensional Flow", *La Houille Blanche*, Vol. 12, 1957, pp. 445-450.

[23] Sheppard, T., Wright, D. S.,"Parameters affecting lateral deformation in slabbing mills", *Metals Technology*, February 1981, pp. 46-57.

[24] W. Johnson, P.B. Mellor, *Engineering Plasticity*, Ellis Horwood Limited,1983

[25] M. J. Luton, J. J. Jonas, *Proc. Int. Conf. Strength Metals Alloys*, 2nd, 1970, pp. 1100-1105.

[26] H. J. McQueen, J. J. Jonas, "Recovery and Recrystallization during High Temperature Deformation", *Plastic Deformation of Materials* Vol. 6, Ed. R. J. Arsenault, 1975, pp. 393-493.

[27] I. Tamura, C. Quchi, T. Tanaka, H. Sekine, *Thermomechanical Processing of High Strength Low Alloy Steel*, 1988.

[28] W. J. McG. Tegart, A. Gittins, "The Hot Deformation of Austenite", *The Hot Deformation of Austenite*, Ed. J. B. Ballance, 1977, pp.1-46.

[29] H. Kudo, "Upper Bound Approach To Metal Forming Processes — To Date And In The Future", *Metal Forming and Impact Mechanics*, Ed. S.R. Reid, Pergamon Press, 1985, pp. 19-45.

[30] H. Kudo, "Some Analytical And Experimental Students of Axi-symmetric cold forging and Extrusion—I", *International Journal of Mechanical Sciences*, Vol. 2, 1960, pp. 102-127.

[31] W. Johnson, J. Inst. Met., Vol. 85, 1956, pp. 403.

[32] L. C. Dodeja, W. Johnson, J. Mech. Phys. Solids, Vol. 5, 1957, pp. 281.

[33] Avitzur, B., *Handbook of Metal-Forming Processes*, John Wiley & Sons, 1983.

[34] Thomsen, E. G., Yang, C. T., Kobayashi, S., *Mechanics of Plastic Deformation in Metal Processing*, the Macmillan Ltd., 1965.

[35] J. Chakrabarty, *Theory of Plastisity*, McGraw-Hill, 1987.

[36] C. Devadas, I. V. Samaradekera, "Heat transfer during hot rolling of steel strip", *Ironmaking and Steelmaking*, Vol.13, No. 6, 1986, pp.311-321.

[37] C. Devadas, "The Prediction of the Evolution of Microstructure During Hot Rolling of Steel Strips", Ph.D. thesis, the University of British Columbia, June 1989.

[38] D. Partington, L. Talbot, "Computer-aided draftiong control in plate rolling", *Hot Working and Forming Processes*, Ed. C. M. Sellers, et al, 1979, pp716-180.

[39] G. F. Bryant, M. O. Heselton, "Roll-Gap Temperature Models for Hot Mills", *Metals Texhmology*, Vol. 9, Dec. 1982, pp.469-477.

[40] F. Hollander, "A model to calculate the complete temperature dsitribution in steel during hot rolling", *The Iron and Steel Institute*, London, 1969, pp.46-78.

[41] Roberts, W. L., *Hot Rolling Of Steel*, Marcel Dekker, INC.1983.

[42] B.I.S.R.A., Ed., *Physical Constants of some Commercial Steels at Elevated Temperatures*, Butterworths, London, 1953, pp.1-38.

[43] J. Woolman, R. A. Mottram, *The Mechanical and Physical Properties of the British Standard EN Steels*, the Macmillan Co., 1964.

[44] R. I. L. Guthrie, *Engineering in Proess Metallurgy*, Oxford Science Publications, 1989.

[45] J. P. Holman, *Heat Transfer*, 6th. edn., McGraw-Hill, 1986.

[46] C. Devadas, I. V. Samaradekera, and E. B. Hawbolt, "The Thermal and Metallurgical State of Steel Strip during Hot Rolling: Part I. Characterization of Heat Transfer", *Metallurgical Transactions*, Vol. 22A, Feb. 1991, pp.307-319.

[47] Ashok Kumar, I. V. Samaradekera, and E. B. Hawbolt, "Roll-bite deformation furing the hot rolling of steel strip", *Journal of Materials Processing Technology*, Vol.30, 1992, pp.91-114.

[48] F. Kreith, W. Z. Black, *Basic Heat Transfer*, Harper and Row, New Youk, 1980.

[49] K. Murata, H. Morise, M. Mitsutsuka, H. Haito, T. Komatsu, and S. Shida, *Trans. Iron Steel Inst. Jpn.*, Vol. 24, (9), 1984, pp.B309.

[50] P. G. Stevens, K. P. Ivens, and P. Harper, *Journal of Iron and Steel Institute*, 1971, Vol. 209, pp.1-11.

[51] M. A. Pinsky, *Introduction to Partial Differential Equations with Application*, McGraw-Hill Book, 1984.

[52] C. M. Sellars, "The Physical Metallurgy of Hot Working", *Hot Working and Forming Processes*, Ed. C. M. Sellers, et al, 1979, pp.3-15.

[53] M. J. Stewart, "Hot Deformation of C-Mn Steels from 1100 to 2200 °F (600 to 1200 °C) with Constant True Strain Rates from 0.5 to 140 s^{-1}", *The Hot Deformation of Austenite*, Ed. J. B. Ballance, 1977, pp.47-67.

[54] S. F. Wong, P. D. Hodgson, P. F. Thomson, "Lead As A Model Material For The Hot Rolling Of Steel", *Mathematical Modelling of Hot Rolling of Steel*, Ed. S. Yue, 1990, pp.281-289.

[55] Chitkara, N. R. and Johnson, W., "Some Experimental Results Concerning Spread in the Rolling of Lead", *Journal of Basic Engineering*, Vol. 88, pp. 489-499, 1966.

[56] Loizou, N. and Sims, R. B., "The Yield Stress of Pure Lead in Compression", *Journal of the Mechanics and Physics of Solids*, Vol. 1, pp. 234 to 243, 1953.

[57] Sims, R. B., "The Calculation of Roll Force and Torque in Hot Rolling Mills", *Proc. Inst. Mech. Engng*, Vol. 168, pp. 191. 1954.

[58] Yang, D. Y., Ryoo, J. S., "An Investigation into the Relationship between Torque and Load in Ring Rolling", *Transactions of ASME, Journal of Engineering for Industry*, Vol. 109, pp. 190-196, Aug. 1987.

[59] Gerald, C. F., Wheatley, P. O., *Applied Numerical Analysis*, 4th edn. 1989.

[60] Hosford, W. F., Caddell, R. M., *METAL FORMING — Mechanics and Metallurgy.* Prentice-Hall, Inc., 1983.

Appendix A

ANALYTICAL SOLUTION TO THE UPPER BOUND EQUATIONS

A.1 The neutral point

Differentiating Eqn.4.39 gives,

$$\frac{\partial Q(x_n)}{\partial w_1} = \frac{V_R t(x_n)}{\sqrt{1+t'(x_n)}} \frac{\partial w(x_n)}{\partial w_1} \tag{A.1}$$

or,

$$\frac{\partial Q(x_n)}{\partial w_1} = \frac{Q(x_n)}{w(x_n)} \frac{\partial w(x_n)}{\partial w_1} \tag{A.2}$$

and

$$\frac{\partial Q(x_n)}{\partial x_n} = Q\left(\frac{1}{t}\frac{\partial t}{\partial x_n} + \frac{1}{w}\frac{\partial w}{\partial x_n} - \frac{t'}{1+t'^2}\frac{\partial t'}{\partial x_n}\right)_{x=x_n} \tag{A.3}$$

A.1.1 The derivative of $\dot{E}_d$ against w_1

From Eq.4.13 and Eq.A.2, the following results,

$$\frac{\partial \dot{E}_d}{\partial w_1} = \frac{1}{w(x_n)} \frac{\partial w(x_n)}{\partial w_1} \dot{E}_d + Q \int_0^l 2\left(\frac{\partial Z_3}{\partial w_1} + \frac{\partial Z_4}{\partial w_1} + \frac{\partial Z_5}{\partial w_1}\right) dx \tag{A.4}$$

where, for the sake of simplicity, define Eq.4.14 as $Z(x) = Z_3(x) + Z_4(x) + Z_5(x)$, and after some manipulations, one may have the following,

$$Z_3(x) = \frac{1}{\alpha}\left(I^2 + \frac{\gamma^2}{3}\right) \ln \frac{\alpha + Z_2}{\beta} \tag{A.5}$$

$$Z_4(x) = \frac{2}{3}\left[Z_2 + \frac{A}{\gamma}(2I_2 + B_2)\right] \tag{A.6}$$

$$Z_5(x) = I^2\left[\left(\frac{2I}{\alpha} - \frac{1}{3}\right)\tan^{-1} D + \frac{I}{\alpha}\left(\frac{1}{3\gamma} - 2\right) t_g\right] \tag{A.7}$$

where, let

$$\gamma = Nt \qquad \alpha = Mw \tag{A.8}$$

$$\beta = \sqrt{I^2 + \gamma^2} \tag{A.9}$$

$$B = \sqrt{I^2 + \alpha^2} \tag{A.10}$$

$$D = \frac{(Z_2 - B)I}{(B + \alpha)\gamma} \tag{A.11}$$

$$Z_2 = \sqrt{B^2 + \gamma^2} \tag{A.12}$$

$$A = \ln \frac{\gamma + Z_2}{B} \tag{A.13}$$

$$t_g = \tan^{-1} \frac{\beta - I}{\gamma} \tag{A.14}$$

and differetiation of Eq.A.8 — A.14 against w_1 results in the following,

$$\frac{\partial \gamma}{\partial w_1} = t\frac{\partial N}{\partial w_1} \tag{A.15}$$

$$\frac{\partial \beta}{\partial w_1} = \frac{1}{2\beta}\left(\frac{\partial I^2}{\partial w_1} + 2\gamma t\frac{\partial N}{\partial w_1}\right) \tag{A.16}$$

$$\frac{\partial \alpha}{\partial w_1} = w\frac{\partial M}{\partial w_1} + M\frac{\partial w}{\partial w_1} \tag{A.17}$$

$$\frac{\partial B^2}{\partial w_1} = \frac{\partial I^2}{\partial w_1} + 2\alpha\frac{\partial \alpha}{\partial w_1} \tag{A.18}$$

$$\frac{\partial Z_2}{\partial w_1} = \frac{1}{2Z_2}\left(\frac{\partial B^2}{\partial w_1} + 2\gamma t\frac{\partial N}{\partial w_1}\right) \tag{A.19}$$

$$\frac{\partial A}{\partial w_1} = \frac{1}{\gamma + Z_2}\left(\frac{\partial \gamma}{\partial w_1} + \frac{\partial Z_2}{\partial w_1}\right) - \frac{1}{B}\frac{\partial B}{\partial w_1} \tag{A.20}$$

$$\frac{\partial t_g}{\partial w_1} = \frac{1}{\gamma^2 + (\beta - I)^2}\left\{(\beta - I)\frac{\partial \gamma}{\partial w_1} - \gamma\left[\frac{\gamma t}{\beta}\frac{\partial N}{\partial w_1} + 2\left(\frac{1}{\beta} - \frac{1}{I}\right)\frac{\partial I^2}{\partial w_1}\right]\right\} \tag{A.21}$$

$$\begin{aligned}\frac{\partial D}{\partial w_1} = {} & \frac{1}{[(B + \alpha)\gamma]^2}\left\{(B + \alpha)\gamma\left[I\left(\frac{\partial Z_2}{\partial w_1} - \frac{\partial B}{\partial w_1}\right) + (Z_2 - B)\frac{\partial I}{\partial w_1}\right]\right. \\ & \left. -(Z_2 - B)I\left[\gamma\left(\frac{\partial B}{\partial w_1} + \frac{\partial \alpha}{\partial w_1}\right) + (B + \alpha)\frac{\partial \gamma}{\partial w_1}\right]\right\}\end{aligned} \tag{A.22}$$

Now, with the help of the Eq.A.8 — A.21, the partial derivative of Eq.A.5, A.6 and

A.7 may be expressed as the following,

$$\frac{\partial Z_3}{\partial w_1} = \frac{1}{\alpha}\left\{-Z_3\frac{\partial \alpha}{\partial w_1} + \left(\frac{\partial I^2}{\partial w_1} + \frac{2}{3}\gamma\frac{\partial \gamma}{\partial w_1}\right)\ln\frac{\alpha + Z_2}{\beta} + \left(I^2 + \frac{\gamma^2}{3}\right)\left[\frac{1}{\alpha + Z_2}\left(\frac{\partial \alpha}{\partial w_1} + \frac{\partial Z_2}{\partial w_1}\right) - \frac{1}{\beta}\frac{\partial \beta}{\partial w_1}\right]\right\} \quad \text{(A.23)}$$

$$\frac{\partial Z_4}{\partial w_1} = \frac{2}{3}\left\{\frac{\partial Z_2}{\partial w_1} + \frac{1}{\gamma}\left[(2I^2 + B^2)\left(\frac{\partial A}{\partial w_1} - \frac{A}{\gamma}\frac{\partial \gamma}{\partial w_1}\right) + A\left(2\frac{\partial I^2}{\partial w_1} + \frac{\partial B^2}{\partial w_1}\right)\right]\right\} \quad \text{(A.24)}$$

$$\frac{\partial Z_5}{\partial w_1} = \frac{Z_5}{I^2}\frac{\partial I^2}{\partial w_1} + I^2\left(\frac{1}{\alpha}\left\{\frac{1}{\alpha}\left(\alpha\frac{\partial I}{\partial w_1} - I\frac{\partial \alpha}{\partial w_1}\right)\left[2\tan^{-1}D + \left(\frac{1}{3\gamma} - 2\right)t_g\right] + I\left[\left(\frac{1}{3\gamma} - 2\right)\frac{\partial t_g}{\partial w_1} - \frac{t_g}{3\gamma^2}\frac{\partial \gamma}{\partial w_1}\right]\right\} - \frac{1}{1 + D^2}\left(\frac{2I}{\alpha} - \frac{1}{3}\right)\frac{\partial D}{\partial w_1}\right) \quad \text{(A.25)}$$

Thus, Eq.A.4 is completely determined.

A.1.2 The derivative of $\dot{E}_f$ against w_1

From Eq.4.20, one may have the following,

$$\frac{\partial \dot{E}_f}{\partial w_1} = mk\left(\frac{\partial Q}{\partial w_1}\int_0^l F(x)\sqrt{1 + t'^2}dx + Q\int_0^l \sqrt{1 + t'^2}\frac{\partial F}{\partial w_1}dx\right) \quad \text{(A.26)}$$

where, let,

$$\varphi_2 = \frac{w'}{wt} \quad \text{(A.27)}$$

$$\varphi_3 = \frac{V_R}{Q} - \frac{\sqrt{1 + t'^2}}{wt} \quad \text{(A.28)}$$

$$\varphi_4 = \sqrt{\varphi_2^2 + \varphi_3^2} \quad \text{(A.29)}$$

then, Eq.4.21 becomes,

$$F(x) = w\left(\varphi_4 + \frac{\varphi_3^2}{\varphi_2} + \ln\frac{\varphi_2 + \varphi_4}{|\varphi_3|}\right) \quad \text{(A.30)}$$

Partial differetiating of Eq.A.27 — A.30 against w_1 results the following,

$$\frac{\partial \varphi_2}{\partial w_1} = \frac{1}{tw^2}\left(w\frac{\partial I^2}{\partial w_1} - w'\frac{\partial w}{\partial w_1}\right) \quad \text{(A.31)}$$

$$\frac{\partial \varphi_3}{\partial w_1} = -\frac{V_R}{Q^2}\frac{\partial Q}{\partial w_1} + \frac{\sqrt{1+t'^2}}{tw^2}\frac{\partial w}{\partial w_1} \tag{A.32}$$

$$\frac{\partial \varphi_4}{\partial w_1} = \frac{1}{\varphi_4}\left(\varphi_2\frac{\partial \varphi_2}{\partial w_1} + \varphi_3\frac{\partial \varphi_3}{\partial w_1}\right) \tag{A.33}$$

$$\begin{aligned}\frac{\partial F}{\partial w_1} = &\left(\varphi_4 + \frac{\varphi_3^2}{\varphi_2} + \ln\frac{\varphi_2+\varphi_4}{|\varphi_3|}\right)\frac{\partial w}{\partial w_1} + w\left\{\left[\frac{1}{\varphi_2+\varphi_4} - \left(\frac{\varphi_3}{\varphi_2}\right)^2\right]\frac{\partial \varphi_2}{\partial w_1}\right. \\ &\left. + \left(2\frac{\varphi_3}{\varphi_2} - \frac{1}{\varphi_3}\right)\frac{\partial \varphi_3}{\partial w_1} + \left(1 + \frac{1}{\varphi_2+\varphi_4}\right)\frac{\partial \varphi_4}{\partial w_1}\right\}\end{aligned} \tag{A.34}$$

note that for Eq.A.30, **when** $\varphi_3 < 0$, $|\varphi_3| = -\varphi_3$, then,

$$\frac{\partial |\varphi_3|}{\partial w_1} = -\frac{\partial \varphi_3}{\partial w_1} \tag{A.35}$$

therefore, we have,

$$\frac{1}{|\varphi_3|}\frac{\partial |\varphi_3|}{\partial w_1} = \frac{1}{\varphi_3}\frac{\partial \varphi_3}{\partial w_1} \tag{A.36}$$

A.1.3 The derivative of $\dot{E}_s$ against w_1

From Eq.4.26 and Eq.4.27, one may have the following,

$$\frac{\partial \dot{E}_s}{\partial w_1} = \dot{E}_s\frac{1}{Q}\frac{\partial Q}{\partial w_1} + kQ\frac{\partial S}{\partial w_1} \tag{A.37}$$

where, let,

$$s = \sqrt{w'^2 + t'^2} \tag{A.38}$$

then,

$$\frac{\partial s}{\partial w_1} = \frac{w'}{s}\frac{\partial w'}{\partial w_1} \tag{A.39}$$

and the following may be obtained with the help of the above two equations,

$$\frac{\partial S}{\partial w_1} = \left\{\frac{4}{3}\frac{w'}{t'}\left(\left[2\ln(t'+s) - \ln w' - \frac{1}{3}\right] + \frac{w'^2}{(t'+s)s} - 2\right)\right.$$

$$+\left(\frac{t'}{w'}\right)^2\left(\frac{1}{w'(w'+s)}+\frac{1}{s}\right)+\frac{2}{3}\ln\frac{s-t'}{w'}-\ln\frac{w'+s}{|t'|}$$
$$-\frac{2}{3}\left(\frac{w'^2}{s(s-t')}-\frac{1}{w'}\right)\Bigg\}_{x=0}\frac{\partial w_0'}{\partial w_1} \tag{A.40}$$

A.1.4 The derivatives of $\dot{E}_d$, $\dot{E}_f$ and $\dot{E}_s$ against x_n

1. From Eq.4.13, one may have the following,

$$\frac{\partial \dot{E}_d}{\partial x_n}=\sqrt{\frac{2}{3}}\sigma\frac{\partial Q}{\partial x_n}\int_0^l Z(x)dx_n \tag{A.41}$$

by substituting Eq.A.3 into the above equation, one may obtain,

$$\frac{\partial \dot{E}_d}{\partial x_n}=\left(\frac{1}{t}\frac{\partial t}{\partial x_n}+\frac{1}{w}\frac{\partial w}{\partial x_n}-\frac{t'}{1+t'^2}\frac{\partial t'}{\partial x_n}\right)_{x=x_n}\dot{E}_d \tag{A.42}$$

2. From Eq.4.20, one may have the following,

$$\frac{\partial \dot{E}_f}{\partial x_n}=mk\left(\frac{\partial Q}{\partial x_n}\int_0^l F(x)\sqrt{1+t'^2}dx+Q\int_0^l\sqrt{1+t'^2}\frac{\partial F}{\partial x_n}dx\right) \tag{A.43}$$

and note that from Eq.A.28 and Eq.A.29,

$$\frac{\partial \varphi_3}{\partial w_1} = -\frac{V_R}{Q^2}\frac{\partial Q}{\partial x_n} \tag{A.44}$$
$$\frac{\partial \varphi_4}{\partial w_1} = -\frac{V_R}{Q^2}\frac{\varphi_3}{\varphi_4}\frac{\partial Q}{\partial x_n} \tag{A.45}$$

Now, with the help of Eq.A.44 and Eq.A.45, partial differentiation of Eq.4.21 results the following,

$$\frac{\partial F}{\partial x_n}=-w\frac{V_R}{Q^2}\left[\frac{\varphi_3}{\varphi_4}\left(1+\frac{1}{\varphi_2+\varphi_4}\right)+\frac{2\varphi_3}{\varphi_2}-\frac{1}{\varphi_3}\right]\frac{\partial Q}{\partial x_n} \tag{A.46}$$

thus, by substituting Eq.A.46 and Eq.A.3 into Eq.A.43, one may obtain,

$$\frac{\partial \dot{E}_f}{\partial x_n} = \left(\frac{1}{t}\frac{\partial t}{\partial x_n}+\frac{1}{w}\frac{\partial w}{\partial x_n}-\frac{t'}{1+t'^2}\frac{\partial t'}{\partial x_n}\right)_{x=x_n}\Bigg\{\dot{E}_f-V_R\int_0^l\sqrt{1+t'^2}\cdot$$
$$\left[\frac{\varphi_3}{\varphi_4}\left(1+\frac{1}{\varphi_2+\varphi_4}\right)+\frac{2\varphi_3}{\varphi_2}-\frac{1}{\varphi_3}\right]dx\Bigg\} \tag{A.47}$$

3. Partial differetiating Eq.4.26 and then using Eq.A.3, one may have the following,

$$\begin{aligned} \frac{\partial \dot{E}_s}{\partial x_n} &= kS\frac{\partial Q}{\partial x_n} \\ &= \left(\frac{1}{t}\frac{\partial t}{\partial x_n} + \frac{1}{w}\frac{\partial w}{\partial x_n} - \frac{t'}{1+t'^2}\frac{\partial t'}{\partial x_n}\right)_{x=x_n} \dot{E}_s \end{aligned} \tag{A.48}$$

Appendix B

TRUE STRESS & STRAIN CORRELATION FOR C-Mn STEELS

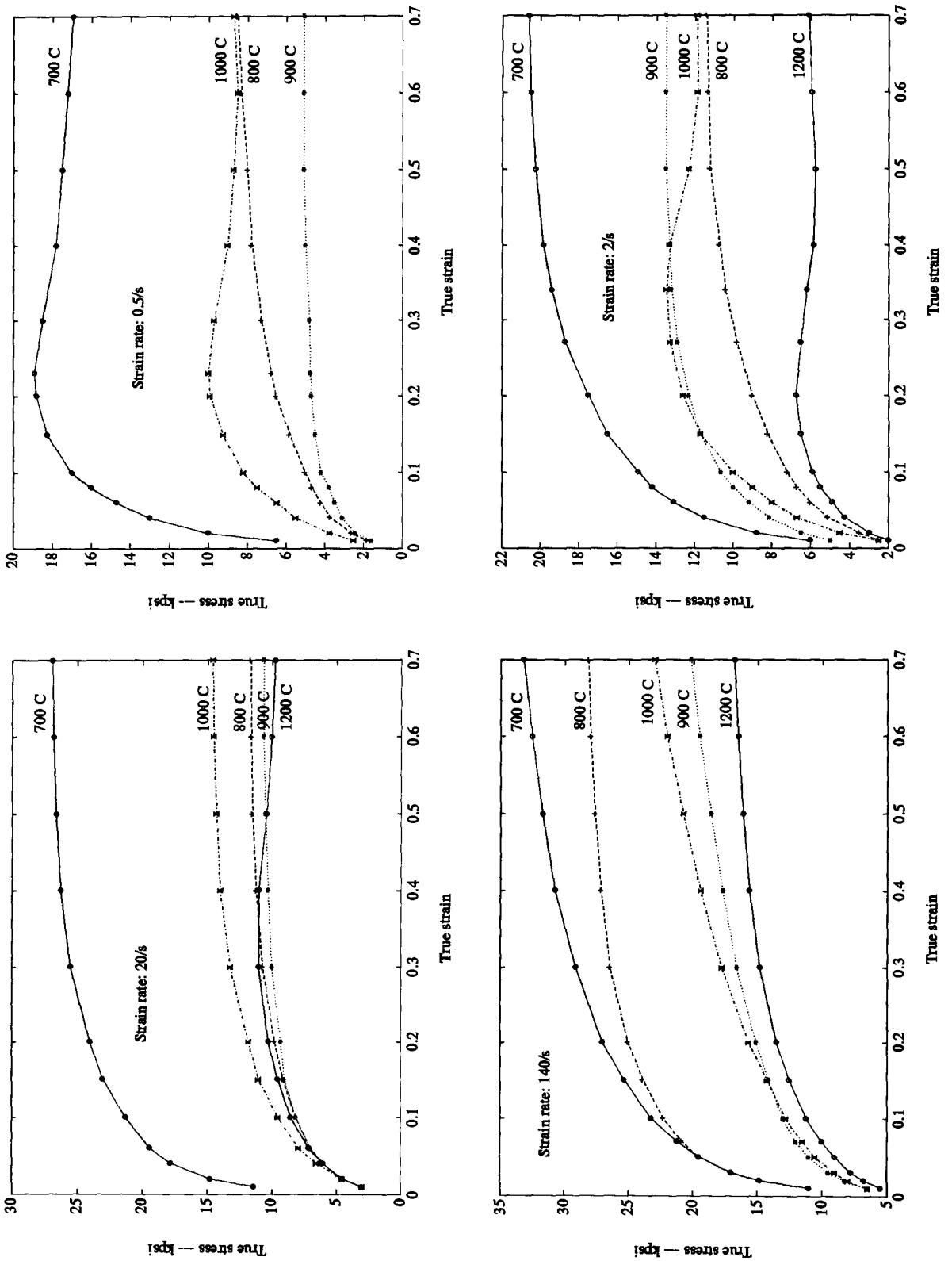

Figure B.1: True- stress and strain relationships for 0.01 C 0.19 Mn steels. *, °, ˣ, + are experimental data

.

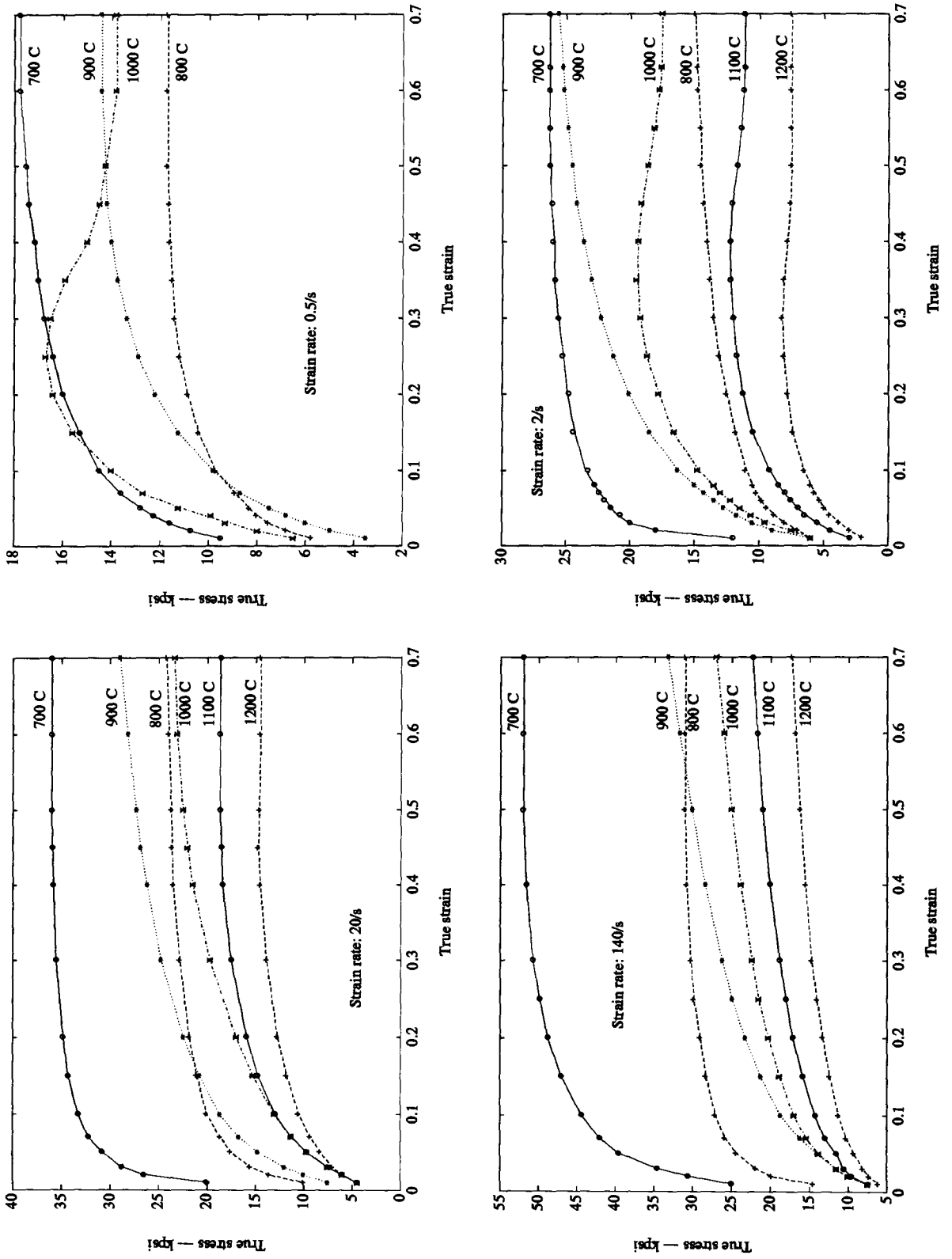

Figure B.2: True- stress and strain relationships for 0.03 C 0.62 Mn steels. *, °, x, + are experimental data

.

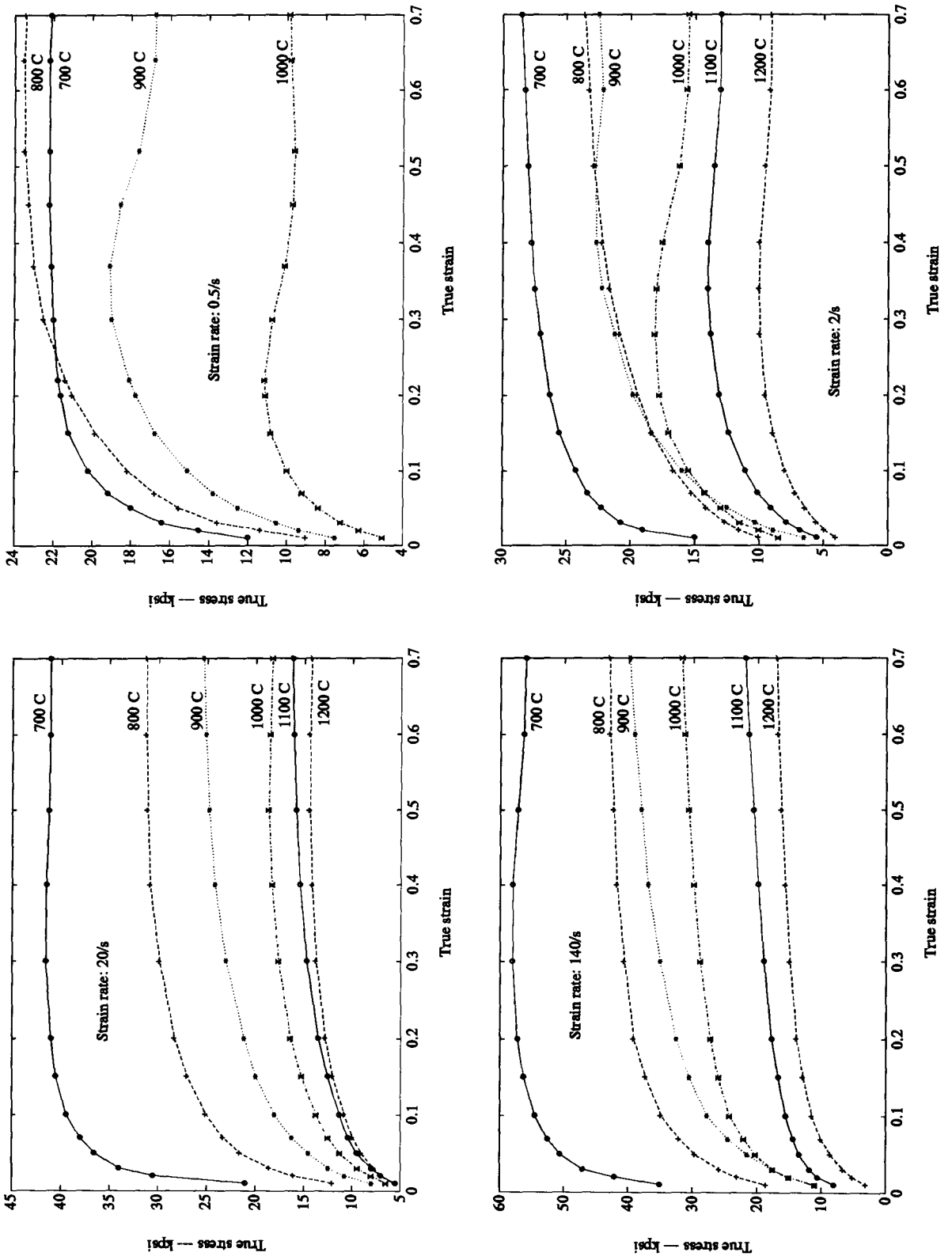

Figure B.3: True- stress and strain relationships for 0.19 C 0.64 Mn steels. *, °, x, + are experimental data

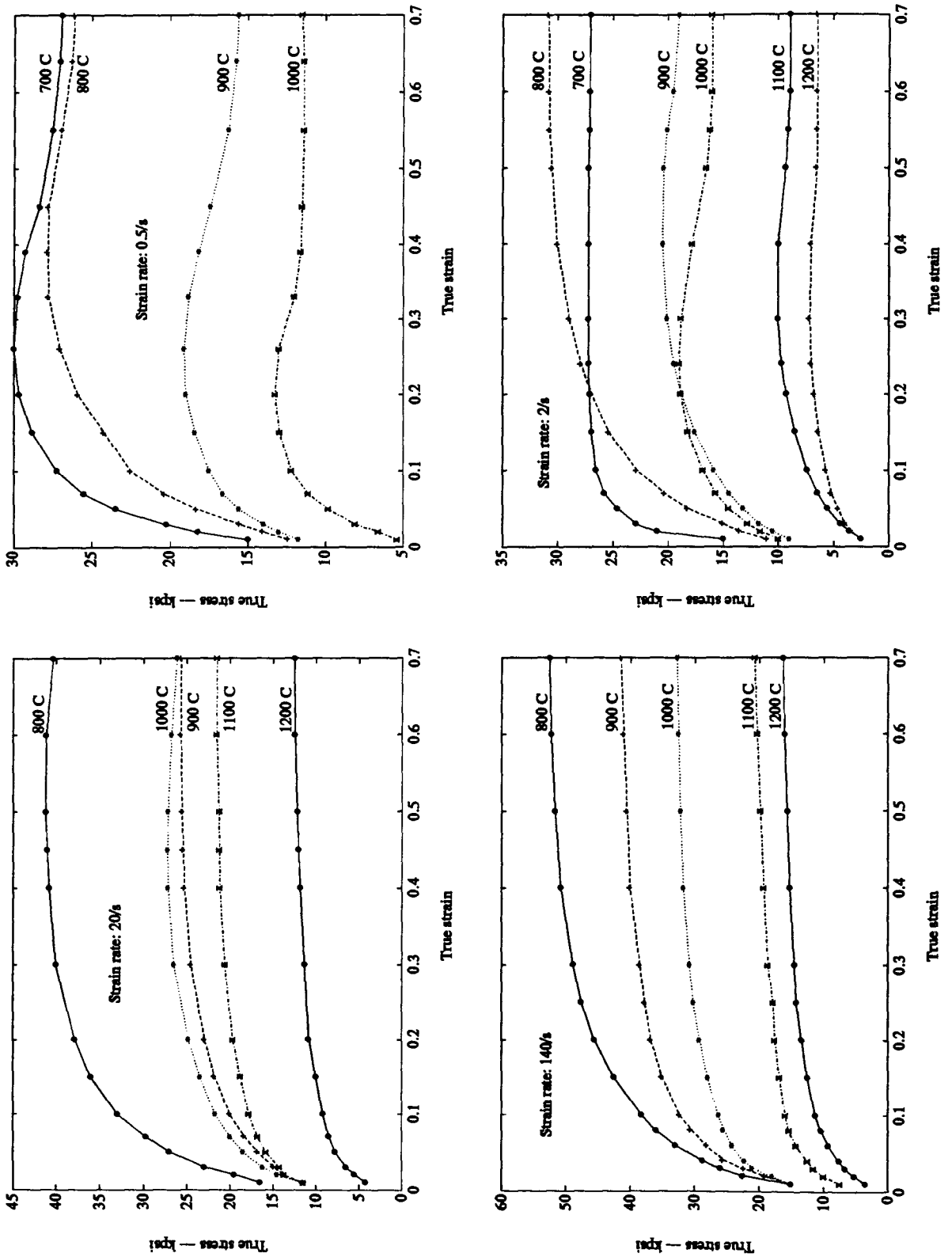

Figure B.4: True- stress and strain relationships for 0.38 C 0.64 Mn steels. *, °, ˣ, + are experimental data

.